MNRAS **473,** 5126–5141 (2018)
Advance Access publication 2017 October 11
doi:10.1093/mnras/stx2647

A search for transit timing variations and orbital decay in WASP-46b

R. Petrucci,[1,2]★† E. Jofré,[1,2]★ L. V. Ferrero,[1,2] V. Cúneo,[1,3] L. Saker,[1,2] F. Lovos,[1,2] M. Gómez[1,2] and P. Mauas[2,3]

[1]*Universidad Nacional de Córdoba, Observatorio Astronómico, Laprida 854, X5000BGR, Córdoba, Argentina*
[2]*Consejo Nacional de Investigaciones Científicas y Técnicas (CONICET), Argentina*
[3]*Instituto de Astronomía y Física del Espacio (IAFE, CONICET-UBA), Av. Inte. Güiraldes 2620, C1428ZAA Buenos Aires, Argentina*

Accepted 2017 October 9. Received 2017 October 5; in original form 2016 June 8

ABSTRACT

We present 12 new transit observations of the exoplanet WASP-46b obtained with the 1.54-m telescope at Estación Astrofísica de Bosque Alegre (EABA, Argentina) and the 0.40-m Horacio Ghielmetti and 2.15-m Jorge Sahade telescopes at Complejo Astronómico El Leoncito (CASLEO, Argentina). We analyse them together with 37 light curves from the literature to re-determine the physical parameters and search for additional planets via transit timing variations (TTVs). We consider the 31 transits with uncertainties in their mid-transit times (e_{T_0}) < 1 min, to perform the first homogeneous study of TTVs for the system, finding a dispersion of $\sigma = 1.66$ min over a 6 yr baseline. Since no periodic variations are found, our interpretation for this relatively high value of σ is that the stellar activity could be affecting the measured mid-transit times. This value of dispersion allows us to rule out the presence of additional bodies with masses larger than 2.3, 4.6, 7 and 9.3 $M_\oplus$ at the first-order mean-motion resonances 2:1, 3:2, 4:3 and 5:4 with the transiting planet, respectively. Despite the 6 yr baseline and a typical light-curve precision of 2×10^{-3}, we find that we cannot significantly demonstrate a slow decrease of the orbital period of WASP-46b. We place a lower limit of $Q_\star > 7 \times 10^3$ on the tidal quality factor and determine that an additional 6 yr baseline is required to rule out $Q_\star < 10^5$.

Key words: techniques: photometric – planets and satellites: individual: WASP-46b – stars: individual: WASP-46.

1 INTRODUCTION

WASP-46b is a Hot Jupiter-like planet orbiting a main-sequence G6 star (V=12.9, K=11.4), discovered by Anderson et al. (2012) from data of the WASP photometric survey (Pollacco et al. 2006) taken during the years 2008 and 2009. Anderson et al. (2012) estimated a planet mass of $M_P = 2.101 \pm 0.073\ M_J$ and a planetary radius of $R_P = 1.310 \pm 0.051\ R_J$ from two transits observed with the 1.2-m Euler and the 0.6-m TRAPPIST telescopes and 16 radial velocity measurements taken with the CORALIE spectrograph. The spectroscopic observations confirm the period of 1.43 d found from the photometric data. The detection of weak emission in the Ca II H+K lines of the CORALIE spectra and a rotational modulation of 16 ± 1 d found in the WASP data confirm that WASP-46 is an active star. Combining this photometric information with the spectroscopically determined rotation velocity, Anderson et al. (2012) inferred an inclination for the stellar spin axis of 41° with respect to the sky plane. They also found an inconsistency between the age of a few Gyr estimated from the lithium abundance and a gyrochronological age of 0.9–1.4 Gyr calculated from the stellar rotation period.

Recently, Maxted, Serenelli & Southworth (2015) used two improved methods to estimate the gyrochronological and isochronal ages of 28 transiting exoplanets. For about half the sample, including WASP-46b, they confirmed the discrepancy found by Anderson et al. (2012) between the age determined by the stellar rotation period and the one obtained by the isochrone fitting. Although there is still no conclusive evidence, the authors suggest as a possible explanation that tidal interaction between the star and the planet has produced a transfer of angular momentum from the planetary orbit to the rotation of the star. This increase in the stellar spin makes the star appear younger than it really is, causing a smaller value for the gyrochronological age than the one measured by using isochrones.

Chen et al. (2014b) observed one secondary eclipse in the g', r', i', z', J, H and K bands simultaneously using the GROND

★ E-mail: romina.petrucci@gmail.com (RP); jofre.emiliano@gmail.com (EJ)

† Visiting Astronomer, Complejo Astronómico El Leoncito operated under agreement between the Consejo Nacional de Investigaciones Científicas y Técnicas de la República Argentina and the National Universities of La Plata, Córdoba and San Juan.

Table 1. Log of our observations.

Date	Telescope	Camera	Filter	Bin-size	X	Exposure-time (s)	N_{obs}	σ(mag)	Aperture radii (px)
2012 July 22	0.40-m THG	U8300	Clear	4 × 4	1.10 → 1.51	20	707	0.0095	1–25
2013 August 11	0.40-m THG	U16M	*R*	2 × 2	1.53 → 1.09	60	215	0.0085	1–25
2013 August 29	1.54-m EABA	U9	*R*	2 × 2	1.11 → 1.53	50	204	0.0025	1–20
2013 October 10	0.40-m THG	U16M	*V*	2 × 2	1.14 → 1.79	50	209	0.0074	1–25
2014 June 30	0.40-m THG	U16M	*R*	2 × 2	1.25 → 1.09 → 1.26	50	314	0.0103	1–5
2014 July 23	1.54-m EABA	U9	*R*	2 × 2	1.11 → 1.09 → 1.26	10	809	0.0034	1–20
2014 August 22	1.54-m EABA	U9	*R*	2 × 2	1.09 → 2.06	55	225	0.0034	1–15
2014 September 14	0.40-m THG	U16M	*R*	2 × 2	1.09 → 1.40	50	184	0.0046	1–25
2014 October 17	1.54-m EABA	U9	*R*	2 × 2	1.09 → 1.54	20	601	0.0050	1–15
2015 September 08	1.54-m EABA	U9	*R*	2 × 2	1.13 → 1.09 → 2.00	40, 50	480	0.0060	1–20
2016 June 10	1.54-m EABA	F16M	*R*	2 × 2	1.86 → 1.09	50	298	0.0028	1–25
2016 July 30	2.15-m CASLEO	Roper	*R*	2 × 2	1.10 → 1.48	40	207	0.0027	1–12

Note. Date is given for the beginning of the transit, X is the airmass change during the observation, N_{obs} is the number of useful exposures[4], σ is the standard deviation of the out-of-transit data points and Aperture radii is the range of aperture sizes in pixels tested by FOTOMCAP.

instrument mounted on the MPG/ESO 2.2-m telescope at La Silla in Chile. They detected thermal emission in the *J*, *H* and *K* bands. The brightness temperatures resulting from these measurements are consistent with a very poor heat redistribution efficiency in the atmosphere of WASP-46b. Also, Zhou et al. (2015) reported the detection of two full secondary eclipses of WASP-46b in the near-IR band K_S with the IRIS2 infrared camera on the 3.9-m Anglo-Australian Telescope. For both eclipses, they measured depth values consistent with the result previously obtained by Chen et al. (2014b).

Kjurkchieva et al. (2015) obtained one complete transit of WASP-46b with a 0.40-m telescope and determined photometric parameters in agreement with those measured by Anderson et al. (2012). Subsequently, Ciceri et al. (2016) observed 10 primary transits of this exoplanet with telescopes of different sizes, ranging from 1.2 to 3.58 m. They determined a slightly lower and more precise value for the planetary radius ($R_P = 1.189 \pm 0.037\ R_J$) than the one reported by Anderson et al. (2012). This result implies that the planet's density is larger than initially thought. These authors also performed the first transit timing variation (TTV) study for this exoplanet. However, the data were not analysed homogeneously since they considered not only the measurements of their mid-transit times but also several values of T_0 directly extracted from the literature. Although their results indicate that a linear ephemeris is not a good fit to the observations, Ciceri et al. (2016) did not find any periodic variation and discarded the presence of a third body gravitationally bound to the system. However, they pointed out the need to acquire more precise mid-transit times and to perform a more homogeneous analysis of these data to firmly establish if there are TTVs or not. Finally, they reported a small difference in the planetary radius measured in the i' and z' bands, that could indicate the presence of water vapor at $\lambda \sim 920$ nm and the absence of potassium at $\lambda \sim 770$ nm.

The work by Ciceri et al. (2016) is the only TTVs study of WASP-46b. However, their results are not conclusive, perhaps due to the fact that not all the mid-transit times used to carry out the analysis were obtained applying the same fitting procedure and error treatment, which means the study is not fully homogeneous. Taking this into account, in this paper, we perform the first homogeneous TTVs study from the analysis of literature data and 12 new transit light curves of WASP-46b collected from the three different telescopes. Furthermore, since a direct implication of the results obtained by Maxted et al. (2015) for WASP-46 is that the planetary orbit would be shrinking, we also investigate the possibility of orbital decay in the system.

This paper is organized as follows: In Section 2, we present our observations and briefly describe the data reduction. In Section 3, we obtain the fundamental stellar parameters and chemical abundances, and we determine the photometric and physical parameters of the system. We also compare the computed values with the results obtained by other authors. In Section 4, we present our study of transit timing variations and the results of the search for orbital decay. The analysis of long-term variations on depth (k) and orbital inclination (i) is also described here. Finally, in Section 5, we present a summary and the conclusions.

2 OBSERVATIONS AND DATA REDUCTION

We observed 12 new transits of WASP-46b between 2012 July and 2016 July. In Table 1, we present a log of our observations. Five complete[1] light curves were obtained with the Horacio Ghielmetti telescope (THG) located at Complejo Astronómico El Leoncito (CASLEO). The THG is an MEADE-RCX 400 telescope with a 0.40-m primary mirror, currently equipped with an Apogee Alta U16M camera and Johnson *UBVRI* filters. Due to a serious electric damage, the U16M was not available for the transit observed during the night of 2012 July 22. Therefore, only in this case, we used a different camera, an Apogee Alta U8300 with 3326 × 2504 5 μm-size pixels, a scale of 0.32 arcsec per pixel, and an FoV = 19 × 14 arcsec^2. The other four light curves were obtained with the Apogee Alta U16M camera with 4096 × 4096 9 μm-size pixels, FoV = 49 ×49 arcsec^2 and a scale of 0.57 arcsec per pixel. For each night, we also took 10 bias and 10 dark frames. Sky flat-field images were not taken since we previously found that flat-fielding correction causes unwanted errors in the photometric data (Petrucci et al. 2013). Averaged bias and median-combined bias-corrected dark frames were subtracted from science images using standard IRAF[2] routines.

Other six light curves were obtained with the 1.54-m telescope located at Estación Astrofísica de Bosque Alegre (EABA). This telescope, operated in Newtonian focus, is currently equipped with

[1] We use the word 'complete' to refer to 'full transit coverage'.

[2] IRAF is distributed by the National Optical Astronomy Observatories, which are operated by the Association of Universities for Research in Astronomy, Inc., under cooperative agreement with the National Science Foundation.

Johnson *UBVRI* filters and a 3070 × 2048 9 μm-size pixels Apogee Alta U9 camera, which provides a scale of 0.25 arcsec per pixel and an FoV = 8 × 12 arcsec^2. We used this configuration to obtain five light curves. However, as a consequence of an electric flaw, the U9 CCD had to be replaced, and for the transit observed during the night of 2016 June 10 we employed a different camera, an Apogee Alta F16M with 4096×4096 9 μm-size pixels, a scale of 0.25 arcsec per pixel and a FoV = 16.8 × 16.8 arcsec^2. Except for one transit, all the light curves were observed complete with their four points of contact visible. The partial transit was acquired during the night of 2014 August 22. In this case, the presence of clouds prevented us from obtaining data before the ingress and between the first and second contact points. A total of 10 bias, 8 dark and 15 dome flat-field frames were taken for each observation. We corrected the EABA images for bias and dark applying the same procedure adopted for the THG ones. These CCD images were divided by the master flat generated as the median combined bias- and dark-corrected flats in the corresponding band.

The remaining transit was obtained during the night of 2016 July 30 with the 2.15-m Jorge Sahade telescope at CASLEO. In this case, we used the Roper Scientific camera with 2048 × 2048 13.5 μm-size pixels, a Johnson *R* filter, and a focal reducer which provided a circular FoV of 9 arcmin radius at a plate scale of 0.45 arcsec per pixel. We took 10 bias and 10 dome flat-field frames. Since the dark current level is quite low (<1 e$^-$/hr/px) dark frames were not taken. We corrected the CASLEO images for bias and then divided by the master flat generated as the median combined bias-corrected flats applying the procedure previously explained.

Contrary to the results obtained for the THG images, in both, CASLEO and EABA images, the flat-fielding correction produces light curves with dispersion values equal or, most of the time, smaller than those from light curves achieved without applying this correction.

Integration times ranging from 10 to 60 s and different CCD bin sizes for the science images were chosen depending on seeing, airmass and atmospheric conditions during the night. The transits' observations were mainly carried out in the *R* filter to decrease the effects of limb-darkening (LD; Mallén-Ornelas et al. 2003). However, one transit was observed with no filter (clear), to increase the signal-to-noise ratio (S/N) without losing temporal resolution. For all the observations, we specially checked the focus of the telescope, to avoid any contamination from the faint star located near WASP-46 at a separation of 17.4 arcsec (Anderson et al. 2012). Central times of the images were recorded in Heliocentric Julian Date based on Coordinated Universal Time (HJD$_{\rm UTC}$).

Instrumental magnitudes ($m_{\rm ins}$) were measured through aperture photometry by using the FOTOMCAP code (Petrucci & Jofré 2016). This is a new quasi-automatic program, written in IRAF, developed to determine precise instrumental magnitudes by applying the method of aperture correction (Howell 1989; Stetson 1990). FOTOMCAP has been demonstrated to significantly improve the results obtained with our previous code FOTOMCC (Petrucci et al. 2013, 2015), allowing not only a decrease in the standard deviation of the light curves but also an increase in the number of useful images to perform the aperture photometry. The main difference between both codes is that FOTOMCC uses the growth curves technique[3] to determine instrumental magnitudes, that sometimes can lead to an incorrect determination of $m_{\rm ins}$ as a consequence of variable background behind the source, incorrect sky background subtraction, or some other errors that affect fainter objects more than brighter ones. FOTOMCAP overcomes these issues by using the method of aperture correction in which a constant is calculated for each image as the median value of the magnitudes obtained from the aperture that allows the highest S/N ($m_{\rm SN}$) minus those from the growth curves technique ($m_{\rm CC}$) for the brightest stars (the range of tested aperture radii is specified in Table 1). Then, the instrumental magnitudes of all the stars are computed by adding this constant or aperture correction to the $m_{\rm SN}$ determined for each star. Differential magnitudes were obtained through the procedure explained in Petrucci et al. (2013), considering as comparison one or several stars of the same field with no indication of variability. It was not possible to use the same reference stars for all the transits because, as mentioned before, observations were carried out with several CCD cameras providing different fields of view. This fact prevented us from taking images of the exactly same stellar field and hence the same comparison stars for all the transits. However, in order to achieve the best light curve for each night, we selected as reference stars those which minimized the scatter in the resulting transit. We present our 12 transits with their best fittings in Fig. 1 and the photometric data in Table 2.

2.1 Literature and public data

We supplemented our 12 transits of WASP-46b with 37 light curves available in the literature and public data bases. We used two transits from Anderson et al. (2012): one observed in an $I + z'$ filter with the 0.60-m TRAPPIST telescope, and the other one acquired with the 1.2-m Euler-Swiss telescope in a Gunn r' filter. Another 20 light curves from Ciceri et al. (2016) were kindly provided to us by the authors. Among them, three were observed with the 1.54-m Danish telescope using a Bessell *R* filter, one with the 3.58-m New Technology Telescope (NTT) in a Gunn g' filter, two with the 1.2-m Euler-Swiss telescope employing a Gunn r' filter, three which were simultaneously observed in the four optical bands $g'r'i'z'$ with the GROND instrument on the 2.2-m MPG telescope, and finally one transit also obtained with GROND but only in the $g'z'$ filters. The remaining light curves were extracted from the Exoplanet Transit Database (ETD)[5] (Poddaný, Brát & Pejcha 2010). We only included 15 complete and clearly visible transits of which 14 were observed without filter and the other one in the *R* filter. Some of these light curves do not include the photometric errors. In those cases, we adopted as error the standard deviation of the out-of-transit data points. These observations were obtained with telescopes whose primary mirrors range from 0.25 to 1.54 m.

3 DETERMINATION OF THE SYSTEM'S PARAMETERS

3.1 Fundamental parameters and chemical abundances

In order to derive the spectroscopic fundamental parameters ($T_{\rm eff}$, log *g*, $v_{\rm turb}$, [Fe/H]) of WASP-46, we obtained five UVES high-resolution spectra from the ESO archive[6] to produce a single spectrum (Fig. 2) with an average S/N ∼ 110 (around 6000 Å).

[3] It consists in the determination of the stellar flux variation as a function of aperture radius, in which the adopted magnitude will be given by the aperture at which the total flux of the source stops increasing.

[5] The ETD can be found at http://var2.astro.cz/ETD/credit.php; see also TRESCA at http://var2.astro.cz/EN/tresca/index.php

[6] http://archive.eso.org/cms.html

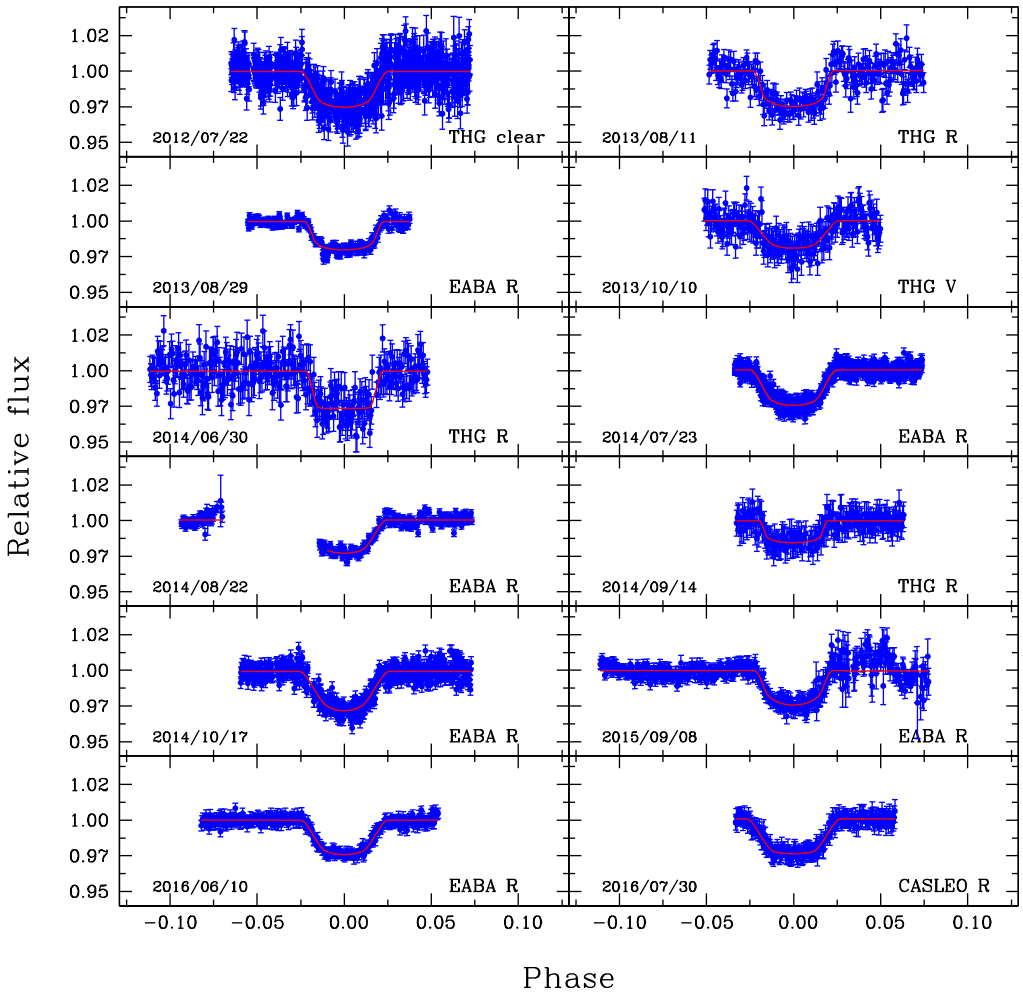

Figure 1. New transit observations presented in this work. Photometric data and their error bars (where errors are the measured ones) are indicated in blue, while the best fittings are marked in solid lines. For each transit the observation date, observatory and filter are also pointed out.

Table 2. Photometry of WASP-46 obtained in this work. This table is available in its entirety in the online journal. A portion is shown here for guidance.

Telescope	BJD_{TDB}	Relative flux	σ_{flux}
0.40-m THG	2456131.721802	1.005	0.008
0.40-m THG	2456131.722057	0.994	0.008
0.40-m THG	2456131.722312	1.004	0.008
0.40-m THG	2456131.722566	0.999	0.008
0.40-m THG	2456131.722821	1.001	0.008
0.40-m THG	2456131.723076	1.006	0.008
0.40-m THG	2456131.723330	0.999	0.008
0.40-m THG	2456131.723585	0.995	0.008
...	...	...	...

We employed the classical procedure, as previously described in Jofré et al. (2015a,b) and Petrucci et al. (2013). Briefly, fundamental parameters are computed from the equivalent widths (EWs) of iron lines (Fe I and Fe II) by imposing excitation and ionization equilibrium and the independence between abundances and EWs, using the FUNDPAR programme (Saffe 2011). FUNDPAR employs the MOOG code (Sneden 1973) and ATLAS9 1D local thermodynamic equilibrium (LTE) model atmospheres (Kurucz 1993). The resulting parameters, along with their statistical uncertainties, are listed in Table 3. Intrinsic uncertainties are based on the scatter of the individual iron abundances from each individual line and the standard deviations in the slopes of the least-squares fits of iron abundances with reduced EWs, excitation and ionization potential (Gonzalez & Vanture 1998). Overall, our parameters are consistent with those reported in the discovery paper (Anderson et al. 2012); however, our T_{eff} value is $\sim$160 K warmer. This discrepancy, within its quoted error, might be related not only to the different technique performed by Anderson et al. to obtain T_{eff} (spectral synthesis of the H_α line) but also due to the higher S/N of our UVES final spectrum compared with their CORALIE spectra of S/N $\sim$ 50. Finally, we also computed the chemical abundances of 14 elements (Na, Mg, Al, Si, Ca, Sc, Ti, V, Cr, Mn, Co, Ni, Y, Ba) from the EWs of several unblended lines using the MOOG programme (abfind driver) as in Jofré et al. (2015a). The computed abundances, relative to the solar values of Anders & Grevesse (1989), along with their dispersions around the mean are also included in Table 3. Our [X/H] values are consistent, within the errors, with those reported by Anderson et al. However, our abundances for all elements (except Mg and Sc) are systematically larger than those of Anderson et al.

Table 3. Fundamental parameters and chemical abundances of WASP-46 derived in this work from UVES spectra.

Parameter (unit)	Value $\pm \sigma$*
$T_{\rm eff}$ (K)	5761 ± 16
log g (cgs)	4.47 ± 0.06
$v_{\rm turb}$ (km s^{-1})	1.10 ± 0.05
[Fe/H]	− 0.25 ± 0.04
[Na/H]	− 0.21 ± 0.08
[Mg/H]	− 0.28 ± 0.1
[Al/H]	− 0.12 ± 0.09
[Si/H]	− 0.25 ± 0.06
[Ca/H]	− 0.20 ± 0.05
[Sc/H]	− 0.21 ± 0.05
[Ti/H]	− 0.15 ± 0.06
[V/H]	− 0.14 ± 0.09
[Cr/H]	− 0.23 ± 0.05
[Mn/H]	− 0.33 ± 0.08
[Co/H]	− 0.20 ± 0.05
[Ni/H]	− 0.24 ± 0.06
[Y/H]	0 ± 0.05
[Ba/H]	0.28 ± 0.05

*For the fundamental parameters, the σ-value represents the intrinsic uncertainties computed following (Gonzalez & Vanture 1998), while for chemical abundances σ is the standard deviation around the mean abundance obtained from all the measured lines.

by ∼0.06 dex, on average. The discrepancies here could be caused by the use of different line list and/or higher errors in the determination of the EWs due to the differences in the quality of the used spectra.

3.2 Photometric parameters

To determine the most precise set of photometric parameters of the system, all the 49 light curves were modelled with the version 34 of the JKTEBOP[7] code (Southworth, Maxted & Smalley 2004). This code uses a Levenberg–Marquardt optimization algorithm to get the model that best fits a transit, and includes Monte Carlo (MC) and bootstrapping routines for error analysis. For each transit, we fitted the inclination (i), the sum of the fractional radii ($\Sigma = r_\star + r_{\rm P}$)[8], the ratio of the fractional radii ($k = r_{\rm P}/r_\star$), the scalefactor (l_0)[9] and the mid-transit time (T_0). This new version of JKTEBOP allows polynomial fitting (up to fifth order) and sine curves simultaneously to the modelling. Therefore, to remove the smooth trends in the light curves caused by differences between the spectral types of the comparison and the exoplanet host-star, differential extinction and stellar activity, we also fitted simultaneously the coefficients of a second-order polynomial. Both orbital period (P) and eccentricity (e) were kept as fixed parameters. For the photometric parameters (i, Σ and k) and P, we adopted as initial values those obtained in Ciceri et al. (2016), while e was assumed to be zero as it was determined in Anderson et al. (2012) and l_0 equals to 1. All the light curves were modelled considering a quadratic LD law. The values of the linear and quadratic LD coefficients q_1 and q_2, respectively, were computed by bilinearly interpolating $T_{\rm eff}$ and log g from the tables of Claret (2000) using the programme JKTLD[10]. However, these tabulations do not provide theoretical LD coefficients for several of the filters used to obtain the transits. In those cases, we adopted the tabulated values of filters with central wavelengths close to those in which the observations were made. Therefore, for the light curves observed in the $g'r'i'z'$ bands with GROND, we used the values of the $g'r'i'z'$ SLOAN filters. For those transits acquired with the Johnson R, the Gunn r' and the Bessell R filters, we used the values tabulated for the Cousin R filter, and for the light curves obtained with no filter we used the average of the values corresponding to the Johnson V and the Cousin R bands. For the transit observed in the Gunn g' band, we used the SLOAN g' filter. Finally, for the observation made in the Cousins I +Sloan z' band, we adopted the values of the Sloan z' filter.

To achieve the best-fitting model for each transit, we examined the results obtained considering: (a) both LD coefficients as free parameters, (b) the linear coefficient slightly perturbed[11] and the quadratic one freely varying, and c) both LD coefficients fixed at their initial values. In almost all the cases, option 'a' gave unphysical results. Among the three possibilities, we choose the option that provided realistic parameters and the lowest value for the χ^2_r. Photometric errors were multiplied by the square-root of the reduced chi-squared of the fit to get $\chi^2_r = 1$. As a final step, we ran 10 000 MC iterations and a residual permutation algorithm that considers the presence of red noise in the photometric data. We adopted as the best-fitting parameters for each transit the median values of the algorithm (MC or residual permutation) that resulted in the largest error, while their errors are the asymmetric uncertainties σ_+ and σ_-, defined by a range of 68.3 per cent values of the selected distribution. In Table 4, we list the parameters for all the light curves.

We also evaluated the quality of each light curve, through the photometric noise rate (PNR), defined by Fulton et al. (2011) as

$$\mathrm{PNR} = \frac{\mathrm{RMS}}{\sqrt{\Gamma}}, \quad (1)$$

where RMS is the standard deviation of the light curve residuals obtained by subtracting the JKTEBOP model from the photometric data, and Γ is the median number of exposures per minute. The red noise level was also estimated through the β parameter, which is defined by Winn et al. (2008) as $\beta = \frac{\sigma_{\rm r}}{\sigma_{\rm N}}$. Here, $\sigma_{\rm r}$ is determined by averaging the residuals into M bins of N points each and computing the standard deviation of the binned residuals and $\sigma_{\rm N}$ represents the expected standard deviation, which in the absence of red noise is defined as

$$\sigma_{\rm N} = \frac{\sigma_1}{\sqrt{N}}\sqrt{\frac{M}{M-1}},$$

where σ_1 is the standard deviation of the unbinned out-of-transit data. Since for WASP-46b the ingress/egress duration of the transit is ∼26 min, residuals were averaged in bins of between 16 and 36 min, and the median value was the adopted red noise factor. In Fig. 3, we show a plot of RMS as a function of the light curve bin size used to calculate the values of β for the 12 new transits. Magenta, blue and green lines represent the measured standard deviations of the binned residuals ($\sigma_{\rm r}$) for the THG, EABA and CASLEO data, respectively, and the black lines correspond to the expected standard

[7] http://www.astro.keele.ac.uk/jkt/codes/jktebop.html

[8] $r_\star = \frac{R_\star}{a}$ and $r_{\rm P} = \frac{R_P}{a}$ are the ratios of the absolute radii of the star and the exoplanet, respectively, to the semimajor axis (a).

[9] This parameter controls the flux level of the out-of-transit data points in the light curves.

[10] http://www.astro.keele.ac.uk/jkt/codes/jktld.html

[11] As indicated in Southworth (2012), the coefficient was perturbed by ± 0.10 around the initial value in the error analysis simulations.

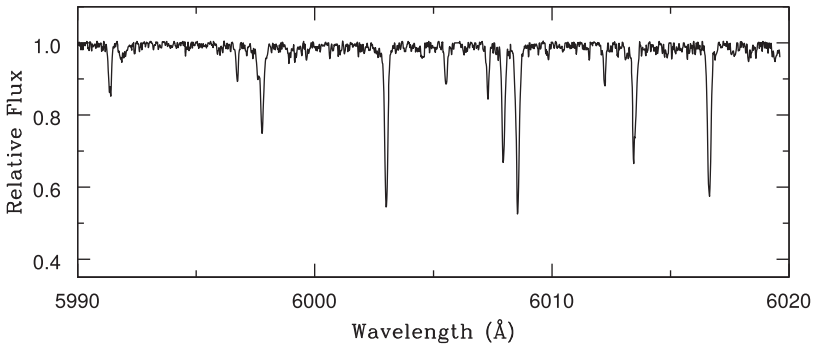

Figure 2. Observed UVES spectrum of WASP-46 in a narrow range around 6000 Å showing several metal lines. This spectrum was used to derive the fundamental stellar parameters and chemical abundances listed in Table 3.

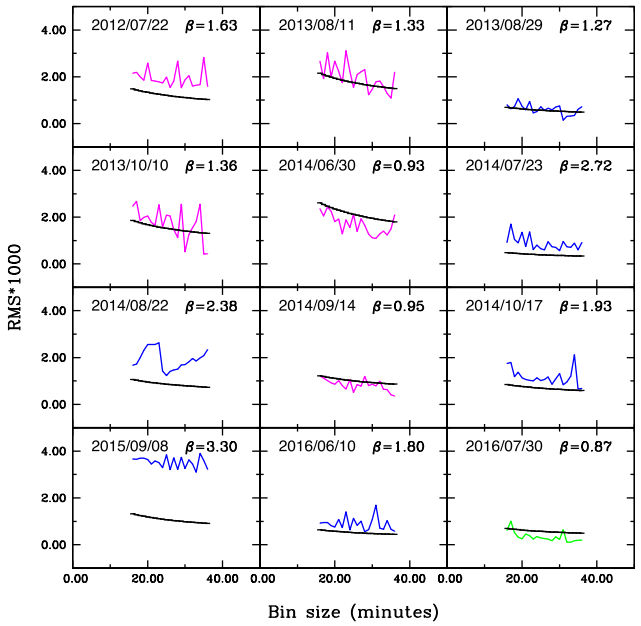

Figure 3. RMS versus light curve bin size used to calculate the values of red noise (β) for the 12 new transits presented in this work. Magenta, blue and green lines represent the measured standard deviations of the binned residuals (σ_r) for the THG, EABA and CASLEO data, respectively, and black lines correspond to the expected standard deviations (σ_N). For each transit, the observation date and the computed red noise are also pointed out.

deviations (σ_N). This plot along with columns 8 and 9 of Table 4 show that our whole sample is composed of light curves of different quality and red noise level.

Taking this into account, to avoid that final photometric parameters being affected by the results obtained from poor quality light curves, we estimated the best set of photometric parameters for the WASP-46 system considering only our most precise complete transits, i.e. light curves with PNR ≤ 3 and $\beta \leq 1.25$[12]. With this criterion we choose a total of 22 light curves[13] (indicated in Table 4 with asterisks) and computed the parameters of the system i, Σ and k as the weighted average of the values determined for each of the selected transits. Parameters uncertainties were calculated as the standard deviation of the sample relative to the number of data. From the 3rd law of *Kepler* and assuming $M_P \ll M_\star$ (where $M_\star$ is the stellar mass), we also estimated the mean stellar density using

$$\rho_\star = \frac{4\pi^2}{GP^2}\left(\frac{1}{r_\star}\right)^3, \quad (2)$$

where G represents the gravitational constant and the value adopted for the orbital period is the one obtained with equation (5) of Section 4. The stellar-density uncertainty was computed through error's propagation. In Table 5, we present our results compared with the values previously obtained by Anderson et al. (2012), Kjurkchieva et al. (2015) and Ciceri et al. (2016). Our parameters agree within the errors with those determined by Anderson et al. (2012), but are slightly different from the ones measured by Ciceri et al. (2016) (except for the value of k which is fully consistent) and those obtained by Kjurkchieva et al. (2015).

3.3 Physical parameters

Physical parameters were calculated using the JKTABSDIM[14] code (Southworth 2009), as explained in Petrucci et al. (2013, 2015). Briefly, this procedure requires as input certain photometric and spectroscopic parameters with their errors. In particular, the best value for the velocity amplitude of the planet is determined by linearly interpolating this parameter between three different stellar models: Y^2 (Demarque et al. 2004), Padova (Girardi et al. 2000) and Teramo (Pietrinferni et al. 2004). For each stellar model, we considered several isochrones comprising the lifetime of the star in the main sequence. In particular, we used isochrones in the ranges 1 Myr–20 Gyr, 63 Myr–18 Gyr and 30 Myr–16 Gyr for the Y^2, Padova and Teramo models, respectively. Then, we calculated the values of $M_\star$, $R_\star$, log $g_\star$, M_P, R_P, a and age with their respective errors.

Planetary surface gravity (g_P), modified equilibrium temperature (T'_{eq}) and Safronov number (Θ) were determined independently of the stellar models, using equation (4) of Southworth, Wheatley & Sams (2007) and equations (5) and (6) of Southworth (2010). The modified equilibrium temperature is similar to the equilibrium temperature (i.e. the temperature that would have a planet if it were supposed as a blackbody heated only by its parent star) when the

[12] These values of PNR and β used to distinguish between high and poor quality transits, were arbitrarily determined from the available light curves to perform this study.

[13] Although the light curves observed the nights of 2011 August 31 and 2012 July 27 have PNR ≤ 3 and $\beta \leq 1.25$, we did not include them in the analysis because they present anomalies during the transit probably produced by the passage of the planet in front of starspots.

[14] http://www.astro.keele.ac.uk/jkt/codes/jktabsdim.html

Table 4. Photometric parameters and quality factors determined for the 49 light curves analysed in this work.

Date	Epoch	i (°)	k	Σ	$r_\star$	r_P	PNR (mmag)	β	Filter	Complete?	Reference
July 19 2010*	3	$81.94^{+0.74}_{-0.79}$	$0.141\,16^{+0.00363}_{-0.00482}$	$0.208\,39^{+0.009\,95}_{-0.009\,19}$	$0.1824^{+0.0090}_{-0.0080}$	$0.025\,74^{+0.001\,08}_{-0.001\,24}$	1.7506	0.5839	Cousins I+Sloan z'	Yes	1
September 10 2010*	40	$81.50^{+0.84}_{-0.35}$	$0.140\,47^{+0.00239}_{-0.00298}$	$0.213\,04^{+0.005\,68}_{-0.012\,44}$	$0.1869^{+0.0045}_{-0.0109}$	$0.026\,16^{+0.000\,89}_{-0.001\,62}$	0.7430	0.9474	Gunn r'	Yes	1
June 09 2011*	231	$83.02^{+1.10}_{-1.54}$	$0.133\,07^{+0.00465}_{-0.00845}$	$0.196\,28^{+0.016\,85}_{-0.013\,64}$	$0.1730^{+0.0151}_{-0.0114}$	$0.023\,22^{+0.001\,82}_{-0.002\,23}$	0.8988	1.0153	Gunn r'	Yes	2
July 14 2011	255	$83.06^{+2.76}_{-1.59}$	$0.152\,76^{+0.01017}_{-0.01084}$	$0.190\,89^{+0.026\,26}_{-0.034\,89}$	$0.1653^{+0.0215}_{-0.0289}$	$0.025\,53^{+0.004\,49}_{-0.005\,98}$	11.4244	0.7333	Clear	Yes	3
August 31 2011	289	$84.45^{+1.13}_{-0.85}$	$0.135\,58^{+0.00407}_{-0.00675}$	$0.178\,25^{+0.012\,93}_{-0.008\,84}$	$0.1569^{+0.0123}_{-0.0076}$	$0.021\,16^{+0.001\,69}_{-0.002\,00}$	0.4862	1.2194	Gunn r'	Yes	2
October 23 2011*	326	$81.95^{+0.37}_{-0.27}$	$0.141\,46^{+0.00151}_{-0.00261}$	$0.205\,32^{+0.002\,80}_{-0.004\,32}$	$0.1797^{+0.0028}_{-0.0037}$	$0.025\,42^{+0.000\,38}_{-0.000\,60}$	0.2023	1.2283	Gunn g'	Yes	2
June 30 2012	501	$84.69^{+5.15}_{-3.78}$	$0.139\,51^{+0.01043}_{-0.01011}$	$0.174\,78^{+0.053\,52}_{-0.033\,28}$	$0.1532^{+0.0445}_{-0.0281}$	$0.021\,68^{+0.008\,06}_{-0.005\,49}$	3.3677	1.3711	Clear	Yes	4
July 02 2012*	503	$82.43^{+0.32}_{-0.39}$	$0.143\,27^{+0.00144}_{-0.00222}$	$0.201\,30^{+0.004\,54}_{-0.004\,14}$	$0.1760^{+0.0042}_{-0.0034}$	$0.025\,26^{+0.000\,82}_{-0.000\,76}$	0.3816	1.0983	Sloan g'	Yes	2
July 02 2012*	503	$82.82^{+0.42}_{-0.51}$	$0.140\,30^{+0.00148}_{-0.00119}$	$0.195\,27^{+0.006\,37}_{-0.004\,49}$	$0.1712^{+0.0056}_{-0.0038}$	$0.024\,15^{+0.000\,81}_{-0.000\,78}$	0.3868	1.2257	Sloan i'	Yes	2
July 02 2012*	503	$82.14^{+0.45}_{-0.37}$	$0.143\,21^{+0.00166}_{-0.00238}$	$0.205\,70^{+0.004\,12}_{-0.005\,21}$	$0.1797^{+0.0039}_{-0.0050}$	$0.025\,76^{+0.000\,62}_{-0.000\,67}$	0.4301	1.0492	Sloan r'	Yes	2
July 02 2012	503	$84.17^{+0.58}_{-0.73}$	$0.137\,14^{+0.00285}_{-0.00252}$	$0.183\,97^{+0.007\,72}_{-0.006\,81}$	$0.1617^{+0.0065}_{-0.0056}$	$0.022\,28^{+0.001\,31}_{-0.001\,20}$	0.5048	1.3005	Sloan z'	Yes	2
July 21 2012*	516	$81.76^{+1.69}_{-1.11}$	$0.140\,06^{+0.00473}_{-0.01475}$	$0.219\,33^{+0.014\,14}_{-0.020\,77}$	$0.1924^{+0.0128}_{-0.0170}$	$0.027\,02^{+0.002\,09}_{-0.003\,94}$	1.8542	0.8195	R	Yes	5
July 22 2012	517	$83.81^{+2.35}_{-2.90}$	$0.146\,53^{+0.01064}_{-0.00716}$	$0.186\,46^{+0.043\,19}_{-0.024\,38}$	$0.1625^{+0.0365}_{-0.0208}$	$0.023\,83^{+0.007\,94}_{-0.003\,97}$	14.4072	1.6334	Clear	Yes	6
July 26 2012	519	$82.68^{+0.92}_{-0.62}$	$0.140\,02^{+0.00281}_{-0.00541}$	$0.194\,67^{+0.007\,15}_{-0.010\,27}$	$0.1705^{+0.0065}_{-0.0088}$	$0.024\,04^{+0.000\,94}_{-0.001\,86}$	1.3726	1.2339	Clear	Yes	7
September 23 2012*	561	$83.52^{+0.52}_{-0.96}$	$0.143\,12^{+0.00393}_{-0.00533}$	$0.188\,59^{+0.011\,33}_{-0.008\,30}$	$0.1652^{+0.0091}_{-0.0073}$	$0.023\,58^{+0.002\,00}_{-0.001\,81}$	0.9753	0.9333	Bessell R	Yes	2
October 16 2012*	577	$83.40^{+0.69}_{-0.57}$	$0.136\,81^{+0.00333}_{-0.00541}$	$0.193\,02^{+0.004\,95}_{-0.007\,04}$	$0.1701^{+0.0039}_{-0.0061}$	$0.023\,21^{+0.001\,05}_{-0.001\,45}$	0.5359	0.7216	Sloan g'	Yes	2
October 16 2012*	577	$82.92^{+0.36}_{-0.43}$	$0.141\,30^{+0.00153}_{-0.00209}$	$0.194\,81^{+0.005\,05}_{-0.004\,32}$	$0.1708^{+0.0043}_{-0.0039}$	$0.024\,23^{+0.000\,62}_{-0.000\,69}$	0.5234	0.9718	Sloan z'	Yes	2
October 27 2012	584	$84.88^{+2.51}_{-1.48}$	$0.139\,70^{+0.00722}_{-0.00704}$	$0.170\,13^{+0.020\,88}_{-0.024\,74}$	$0.1494^{+0.0175}_{-0.0212}$	$0.021\,14^{+0.003\,67}_{-0.003\,73}$	3.0259	0.9244	Clear	Yes	8
April 24 2013*	710	$83.49^{+0.88}_{-0.71}$	$0.130\,21^{+0.01410}_{-0.00451}$	$0.188\,76^{+0.017\,84}_{-0.009\,67}$	$0.1663^{+0.0170}_{-0.0094}$	$0.022\,63^{+0.001\,66}_{-0.001\,45}$	0.3543	0.8296	Sloan g'	Yes	2
April 24 2013	710	$82.89^{+0.57}_{-0.32}$	$0.141\,76^{+0.00206}_{-0.00291}$	$0.191\,98^{+0.004\,98}_{-0.007\,63}$	$0.1681^{+0.0048}_{-0.0070}$	$0.023\,88^{+0.000\,64}_{-0.001\,11}$	0.5557	1.2993	Sloan i'	Yes	2
April 24 2013	710	$81.74^{+0.44}_{-0.36}$	$0.146\,44^{+0.00223}_{-0.00338}$	$0.211\,86^{+0.004\,41}_{-0.006\,60}$	$0.1848^{+0.0041}_{-0.0062}$	$0.026\,91^{+0.000\,77}_{-0.000\,88}$	0.3502	1.4976	Sloan r'	Yes	2
April 24 2013	710	$85.12^{+0.84}_{-0.82}$	$0.157\,40^{+0.00682}_{-0.00542}$	$0.168\,04^{+0.007\,15}_{-0.008\,16}$	$0.1452^{+0.0070}_{-0.0077}$	$0.023\,14^{+0.000\,75}_{-0.001\,32}$	0.4398	1.3203	Sloan z'	Yes	2
June 16 2013*	747	$82.45^{+0.68}_{-0.57}$	$0.140\,01^{+0.00153}_{-0.00536}$	$0.200\,49^{+0.007\,67}_{-0.010\,08}$	$0.1758^{+0.0076}_{-0.0086}$	$0.024\,63^{+0.001\,12}_{-0.001\,23}$	0.5489	0.8654	Sloan g'	Yes	2
June 16 2013*	747	$83.67^{+0.65}_{-0.72}$	$0.138\,13^{+0.00248}_{-0.00241}$	$0.182\,13^{+0.009\,02}_{-0.009\,96}$	$0.1599^{+0.0079}_{-0.0085}$	$0.022\,15^{+0.001\,22}_{-0.001\,54}$	0.7442	0.8504	Sloan i'	Yes	2
June 16 2013*	747	$81.89^{+0.43}_{-0.59}$	$0.136\,53^{+0.00332}_{-0.00293}$	$0.205\,42^{+0.007\,47}_{-0.006\,73}$	$0.1806^{+0.0070}_{-0.0065}$	$0.024\,73^{+0.001\,13}_{-0.001\,11}$	0.7624	1.0033	Sloan r'	Yes	2
June 16 2013	747	$83.42^{+2.80}_{-1.68}$	$0.135\,87^{+0.00842}_{-0.01751}$	$0.196\,49^{+0.015\,29}_{-0.027\,36}$	$0.1723^{+0.0141}_{-0.0239}$	$0.023\,38^{+0.002\,68}_{-0.004\,45}$	1.0829	1.6236	Sloan z'	Yes	2
August 05 2013*	782	$82.84^{+0.55}_{-0.73}$	$0.133\,05^{+0.01271}_{-0.00589}$	$0.201\,66^{+0.015\,08}_{-0.009\,40}$	$0.1776^{+0.0146}_{-0.0094}$	$0.024\,16^{+0.001\,18}_{-0.001\,02}$	0.6023	0.8213	Bessell R	Yes	2
August 05 2013*	782	$82.30^{+1.39}_{-1.19}$	$0.149\,98^{+0.00682}_{-0.00671}$	$0.207\,18^{+0.021\,77}_{-0.015\,89}$	$0.1801^{+0.0175}_{-0.0131}$	$0.027\,01^{+0.003\,68}_{-0.002\,40}$	2.9548	1.0688	Clear	Yes	4
August 11 2013	786	$87.08^{+2.82}_{-5.38}$	$0.137\,25^{+0.01154}_{-0.02501}$	$0.163\,41^{+0.045\,04}_{-0.021\,08}$	$0.1440^{+0.0403}_{-0.0192}$	$0.019\,18^{+0.005\,28}_{-0.002\,44}$	7.0480	1.3326	Jhonson R	Yes	6
August 16 2013	789	$84.52^{+3.77}_{-2.52}$	$0.139\,68^{+0.00637}_{-0.01932}$	$0.175\,21^{+0.031\,55}_{-0.025\,55}$	$0.1538^{+0.0284}_{-0.0219}$	$0.021\,52^{+0.002\,59}_{-0.005\,17}$	4.9027	0.8861	Clear	Yes	4
August 28 2013*	798	$82.66^{+0.59}_{-0.49}$	$0.140\,33^{+0.00149}_{-0.00215}$	$0.196\,41^{+0.005\,54}_{-0.006\,19}$	$0.1722^{+0.0051}_{-0.0053}$	$0.024\,25^{+0.000\,65}_{-0.001\,05}$	0.6097	1.1871	Bessell R	Yes	2
August 28 2013	798	$86.33^{+3.55}_{-2.41}$	$0.126\,91^{+0.00492}_{-0.00378}$	$0.154\,59^{+0.025\,22}_{-0.015\,78}$	$0.1374^{+0.0216}_{-0.0138}$	$0.017\,22^{+0.002\,36}_{-0.002\,08}$	2.8194	1.2699	Jhonson R	Yes	9
October 10 2013	828	$81.50^{+4.71}_{-2.09}$	$0.132\,07^{+0.01253}_{-0.01339}$	$0.216\,74^{+0.031\,40}_{-0.065\,31}$	$0.1910^{+0.0255}_{-0.0561}$	$0.025\,23^{+0.006\,03}_{-0.009\,45}$	7.1662	1.3588	Jhonson V	Yes	6
October 24 2013	837	$84.12^{+1.30}_{-1.44}$	$0.137\,09^{+0.00443}_{-0.00834}$	$0.180\,78^{+0.018\,09}_{-0.017\,28}$	$0.1585^{+0.0162}_{-0.0143}$	$0.021\,63^{+0.002\,88}_{-0.002\,80}$	3.1192	1.1956	Clear	Yes	10
November 13 2013	851	$83.53^{+1.17}_{-1.20}$	$0.134\,52^{+0.00583}_{-0.00394}$	$0.187\,49^{+0.016\,46}_{-0.017\,49}$	$0.1642^{+0.0151}_{-0.0139}$	$0.022\,14^{+0.002\,84}_{-0.002\,41}$	3.0851	1.6816	Clear	Yes	10
June 30 2014	1012	$86.53^{+3.38}_{-4.84}$	$0.151\,61^{+0.00666}_{-0.02164}$	$0.150\,54^{+0.053\,71}_{-0.017\,25}$	$0.1310^{+0.0494}_{-0.0156}$	$0.019\,59^{+0.004\,37}_{-0.002\,19}$	9.7489	0.9315	Jhonson R	Yes	6
July 23 2014	1028	$82.96^{+0.89}_{-0.83}$	$0.147\,54^{+0.00417}_{-0.00567}$	$0.197\,18^{+0.010\,67}_{-0.013\,89}$	$0.1716^{+0.0096}_{-0.0118}$	$0.025\,36^{+0.001\,81}_{-0.002\,19}$	6.7399	2.7261	Jhonson R	Yes	9
August 13 2014	1042	$79.55^{+1.79}_{-3.38}$	$0.170\,84^{+0.21292}_{-0.01595}$	$0.244\,01^{+0.040\,51}_{-0.029\,44}$	$0.1995^{+0.0166}_{-0.0174}$	$0.036\,48^{+0.040\,56}_{-0.007\,55}$	3.4746	1.3159	Clear	Yes	11
August 16 2014*	1044	$82.30^{+1.62}_{-1.23}$	$0.141\,71^{+0.00907}_{-0.01431}$	$0.204\,61^{+0.022\,00}_{-0.021\,10}$	$0.1791^{+0.0197}_{-0.0178}$	$0.025\,30^{+0.003\,28}_{-0.003\,48}$	2.6317	0.5278	Clear	Yes	11
August 22 2014	1049	$82.28^{+1.84}_{-2.23}$	$0.147\,20^{+0.00942}_{-0.01137}$	$0.202\,43^{+0.036\,89}_{-0.024\,23}$	$0.1764^{+0.0310}_{-0.0208}$	$0.025\,68^{+0.006\,43}_{-0.003\,69}$	2.7173	2.3797	Jhonson R	No	9
September 14 2014	1065	$88.93^{+0.97}_{-7.25}$	$0.139\,04^{+0.01337}_{-0.01112}$	$0.179\,71^{+0.020\,03}_{-0.014\,47}$	$0.1575^{+0.0191}_{-0.0113}$	$0.022\,11^{+0.002\,75}_{-0.003\,58}$	4.3655	0.9495	Jhonson R	Yes	6
October 12 2014	1084	$84.11^{+2.57}_{-1.34}$	$0.164\,48^{+0.00677}_{-0.00962}$	$0.178\,12^{+0.019\,59}_{-0.030\,41}$	$0.1525^{+0.0170}_{-0.0245}$	$0.025\,20^{+0.003\,36}_{-0.005\,57}$	4.0209	0.9035	Clear	Yes	4
October 17 2014	1088	$81.73^{+1.34}_{-1.20}$	$0.153\,91^{+0.00753}_{-0.01176}$	$0.222\,23^{+0.023\,10}_{-0.022\,08}$	$0.1926^{+0.0197}_{-0.0189}$	$0.029\,43^{+0.003\,51}_{-0.003\,43}$	7.2769	1.9345	Jhonson R	Yes	9
September 08 2015	1316	$85.49^{+4.34}_{-2.68}$	$0.131\,64^{+0.02183}_{-0.01697}$	$0.184\,94^{+0.052\,26}_{-0.039\,86}$	$0.1623^{+0.0454}_{-0.0345}$	$0.021\,37^{+0.006\,91}_{-0.005\,63}$	6.4132	3.3073	Jhonson R	Yes	9
September 28 2015	1330	$82.10^{+1.66}_{-2.57}$	$0.238\,12^{+0.06121}_{-0.03058}$	$0.228\,61^{+0.034\,27}_{-0.030\,46}$	$0.1858^{+0.0146}_{-0.0248}$	$0.043\,46^{+0.016\,04}_{-0.008\,94}$	7.5577	0.9996	Clear	Yes	11
June 10 2016	1509	$82.25^{+0.68}_{-0.57}$	$0.146\,93^{+0.00474}_{-0.00312}$	$0.204\,36^{+0.009\,06}_{-0.0101}$	$0.178\,06^{+0.007\,54}_{-0.008\,45}$	$0.026\,22^{+0.001\,71}_{-0.001\,56}$	2.6218	1.8010	Jhonson R	Yes	9
July 22 2016*	1539	$83.78^{+0.96}_{-1.44}$	$0.134\,41^{+0.00275}_{-0.00501}$	$0.181\,19^{+0.016\,29}_{-0.013\,03}$	$0.159\,61^{+0.013\,69}_{-0.011\,01}$	$0.021\,49^{+0.002\,21}_{-0.001\,78}$	2.7467	0.9531	Clear	Yes	12
July 30 2016*	1544	$81.6^{+1.75}_{-1.29}$	$0.146\,53^{+0.00379}_{-0.00732}$	$0.219\,95^{+0.013\,87}_{-0.021\,19}$	$0.191\,75^{+0.012\,66}_{-0.0179}$	$0.027\,83^{+0.002}_{-0.003\,21}$	2.8966	0.8727	Jhonson R	Yes	13
August 08 2016*	1551	$82.73^{+0.41}_{-0.43}$	$0.143\,14^{+0.00383}_{-0.00293}$	$0.199\,51^{+0.006\,57}_{-0.006\,67}$	$0.174\,26^{+0.005\,82}_{-0.005\,67}$	$0.024\,89^{+0.001\,27}_{-0.001}$	2.1361	0.8638	Clear	Yes	14

Column 2: values of the parameter Epoch, which represents the number of transits since the minimum reference time shown in equation (4). Columns 3–7: values of the derived photometric parameters orbital inclination (i), ratio of the fractional radii (k), sum of the fractional radii (Σ), ratio of the absolute stellar radius to the semimajor axis ($r_\star$) and ratio of the absolute planetary radius to the semimajor axis (r_P) and their errors. Column 8: Photon noise rate. Column 9: median value for the red noise.

References. (1) Anderson et al. (2012); (2) Ciceri et al. (2016); (3) Curtis I. (ETD); (4) Evans P. (ETD); (5) Sauer T. (ETD); (6) This work (THG); (7) Schneiter M, Colazo C. (ETD); (8) Colazo C. A. (ETD); (9) This work (EABA); (10) Schneiter M., Villarreal C., Colazo C. (ETD); (11) Mašek M., Hoňková K., Juryšek J. (ETD); (12) Villarreal C., Quiñones C. (ETD); (13) This work (CASLEO); and (14) Quiñones C., Melia R., Colazo C. (ETD).

Note. Asterisks indicate the transits used to calculate the final values of i, k, Σ, $r_\star$ and r_P.

Table 5. Photometric parameters derived in this work along with the values previously determined by Anderson et al. (2012), Kjurkchieva et al. (2015) and Ciceri et al. (2016).

Parameter	This work	Ciceri et al. (2016)	Kjurkchieva et al. (2015)	Anderson et al. (2012)
Orbital inclination, i (°)	82.53 ± 0.13	82.80 ± 0.17	82.015 ± 0.005	82.63 ± 0.38
Ratio of fractional radii, k	0.140 74 ± 0.000 68	0.140 75 ± 0.000 35	–	0.1468 ± 0.0017
Sum of fractional radii, $r_\star$+r_P	0.1999 ± 0.0016	0.1950 ± 0.0013	–	0.1992 ± 0.0059
Stellar fractional radius, $r_\star$	0.1750 ± 0.0014	0.1709 ± 0.0011	0.179 ± 0.001	0.1742 ± 0.0057
Planetary fractional radius, r_P	0.024 74 ± 0.000 24	0.024 03 ± 0.000 21	0.027 25 ± 0.000 05	0.0250 ± 0.0010
Stellar density, $\rho_\star$ ($\rho_\odot$)	1.220 ± 0.031	1.310 ± 0.025	–	1.24 ± 0.10

Note. Photometric errors of Kjurkchieva et al. (2015) might be underestimated since they are just the formal values measured by the code used to fit the transits.

Table 6. Physical parameters derived in this work along with the values previously determined by Anderson et al. (2012) and Ciceri et al. (2016).

Parameter	This work	Ciceri et al. (2016)	Anderson et al. (2012)
Stellar mass, $M_\star$ ($M_\odot$)	0.907 ± 0.033	0.828 ± 0.067 ± 0.036	0.956 ± 0.034
Stellar radius, $R_\star$ ($R_\odot$)	0.905 ± 0.013	0.858 ± 0.024 ± 0.013	0.917 ± 0.028
Planetary mass, M_P (M_J)	2.031 ± 0.072	1.91 ± 0.11 ± 0.06	2.101 ± 0.073
Planetary radius, R_P (R_J)	1.244 ± 0.019	1.174 ± 0.033 ± 0.017	1.310 ± 0.051
Planetary surface gravity, g_P (m s^{-2})	32.4 ± 3.0	34.3 ± 1.1	$28.0^{+2.2}_{-2.0}$
Planetary density, ρ_P (ρ_J)	1.054 ± 0.062	1.103 ± 0.050 ± 0.016	0.94 ± 0.11
Planetary modified equilibrium temperature, T'_{eq} (K)	1704 ± 18	1636 ± 44	1654 ± 50
Safronov number, Θ	0.0863 ± 0.0045	0.0916 ± 0.0035 ± 0.0014	–
Semimajor axis, a (AU)	0.02407 ± 0.00029	0.023 35 ± 0.000 63 ± 0.000 34	0.024 48 ± 0.000 28
Age (Gyr)	3.6 ± 1.9	$9.6^{+3.4+1.4}_{-4.2-3.5}$	0.9–1.4[a] Gyr

[a]This is the value obtained by Anderson et al. (2012) for the gyrochronological age.
Note. The modified equilibrium temperature is similar to the equilibrium temperature (i.e. the temperature that would have a planet if it were supposed as a blackbody heated only by its parent star) when the Bond albedo, A, is considered equal to 1 − 4F, where F is a heat redistribution factor; while the Safronov number is an indicator of the efficiency with which a planet scatters other bodies (Fressin et al. 2009).

Bond albedo, A, is considered equal to 1 − 4F, where F is a heat redistribution factor; while the Safronov number is an indicator of the efficiency with which a planet scatters other bodies (Fressin, Guillot & Nesta 2009). Parameters uncertainties were calculated from the propagation of errors. In Table 6, we present our results along with the values previously obtained by Anderson et al. (2012) and Ciceri et al. (2016). It can be seen that, in general, our parameters are in good agreement with those computed in previous works. However, in the particular case of the planetary radius, our estimation is similar within the error to the value presented in the discovery paper (Anderson et al. 2012) but slightly larger than the result obtained by Ciceri et al. (2016). Finally, although the density calculated in this work for WASP-46b agrees within errors with the ones previously determined, our value indicates that the planet is more dense than pointed out by Anderson et al. (2012) but not as much as claimed by Ciceri et al. (2016).

4 ANALYSIS OF TTVS

We used the mathematical transformations described in Eastman, Siverd & Gaudi (2010) to convert measured times into BJD_{TDB}. To carry out a fully homogeneous analysis of TTVs, mid-transit times were determined by fitting all the 49 light curves with the JKTEBOP code. Since T_0 is not correlated with the photometric parameters, each individual light curve was modelled by assuming T_0, l_0, and the coefficients of the polynomial to fit the out-of-transit data points as the only free variables. As initial values for i, k and Σ, we assumed those determined in Section 3.2. We ran 10 000 MC iterations and a residual permutation algorithm. For the mid-transit times, we finally adopted the mean values given by the best JKTEBOP fit to each light curve, and the errors were assumed as the asymmetric uncertainties σ_+ and σ_- of the algorithm (MC or residual permutation) that resulted in the largest error. These results are shown in Table 7. In our sample, we have independent observations of the same transit for two different epochs. Although the values of T_0 do not agree with each other, even considering errors, it is important to mention that, in both cases, one of the transits has much higher quality than the other (PNR ∼ 0.6 compared to PNR ∼ 3). As we show in the next paragraphs, larger values of PNR imply less accurate values of T_0, which should explain the discrepancy. In the following analysis, we treated each measurement separately.

We have excluded four light curves from the ephemeris computation. The transit observed during the night of 2014 August 22 was not considered because it is partial, while those transits acquired the nights of 2011 August 31, 2012 July 26, and the one obtained in the Sloan z' filter the night of 2012 July 2 were not included because they show some visible anomalies during the transit. We suspect that these asymmetries could be caused by stellar activity or simply by bad weather conditions (thin clouds, fog, etc.). We computed new ephemeris fitting a linear model to the remaining 45 light curves through least-squares weighted by the mid-transit times uncertainties. Considering these data we obtained

$$T_0(E) = 2455392.31738(36)\mathrm{BJD_{TDB}} + E \times 1.430\,371\,26(50), \quad (3)$$

where E represents the epoch, i.e. the number of transits since the minimum reference time. The errors for the orbital period and minimum reference time correspond to the last digits and were computed from the covariance matrix of the fit. We obtained a $\chi^2_r = 13.17$ that implies that a linear ephemeris does not properly represent the mid-transit times behaviour. In the bottom panel of Fig. 4, we plot O−C versus Epoch, where the O−C values shown in the y-axis are the observed mid-transit times T_0 minus the ones predicted using the ephemeris given by equation (3). Here, dashed lines represent ±σ, i.e. the standard deviation of the sample (σ = 2.61 min). In this

Table 7. Mid-transit times calculated from the procedure explained in Section 4.

Epoch	T_0 (BJD$_{TDB}$)	e_{T_0}
3	2455396.607854	0.000 618
40	2455449.530824	0.000 265
231	2455722.731779	0.000 229
255	2455757.061951	0.000 941
289*	2455805.693185	0.000 205
326	2455858.618330	0.000 089
501	2456108.927705	0.000 941
503	2456111.794218	0.000 159
503	2456111.794128	0.000 120
503	2456111.794240	0.000 150
503*	2456111.794547	0.000 167
516	2456130.388946	0.000 415
517	2456131.814561	0.001 116
519*	2456134.676108	0.000 289
561	2456194.759161	0.000 270
577	2456217.641274	0.000 147
577	2456217.641561	0.000 132
584	2456227.655743	0.000 604
710	2456407.880958	0.000 154
710	2456407.880849	0.000 176
710	2456407.881483	0.000 282
710	2456407.881594	0.000 426
747	2456460.805257	0.000 173
747	2456460.805193	0.000 263
747	2456460.804500	0.000 243
747	2456460.805467	0.000 643
782	2456510.868182	0.000 602
782	2456510.866993	0.000 150
786	2456516.586674	0.001 191
789	2456520.880123	0.000 637
798	2456533.752605	0.000 707
798	2456533.754796	0.000 152
828	2456576.662886	0.001 087
837	2456589.541970	0.000 899
851	2456609.566526	0.000 426
1012	2456839.854400	0.001 226
1028	2456862.740854	0.000 482
1042	2456882.765657	0.000 726
1044	2456885.624290	0.000 529
1049*	2456892.778598	0.000 957
1065	2456915.660396	0.001 232
1084	2456942.838802	0.000 784
1088	2456948.563838	0.000 740
1316	2457274.684578	0.001 838
1330	2457294.708862	0.001 400
1509	2457550.747972	0.000 306
1539	2457593.656923	0.000 242
1544	2457600.809853	0.000 393
1551	2457610.822857	0.000 203

Note. Asterisks indicate the transits excluded from the calculation of ephemeris.

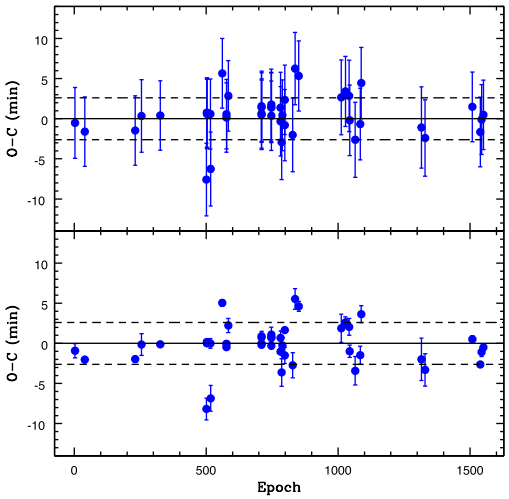

Figure 4. O−C data points versus Epoch considering the 45 light curves without anomalies in their transits. The O−C values are the observed mid-transit times minus the mid-transit times predicted using a specific ephemeris equation, while Epoch represents the number of transits since the minimum reference time shown in the same equation. Bottom panel: O−C values obtained from the ephemeris given by equation (3). Upper panel: O−C values obtained from the ephemeris given by equation (5). Here, the error bars include the extra variance component of 4.32 min, added in quadrature to the mid-transit times errors, which was computed from a maximum-likelihood approach. In both panels, dashed lines indicate $\pm\sigma$ ($\sigma = 2.61$ min) that represents the standard deviation of the data.

$$\ln(\mathcal{L}) = -\frac{n}{2}\ln(2\pi) - \frac{1}{2}\chi^2 - \frac{1}{2}\sum_{i=1}^{n}\ln\left(e_{T_0}^2 + \sigma_s^2\right), \quad (4)$$

where χ^2 is the chi-squared value of $n = 45$ data points with uncertainties e_{T_0}. Through this approach, we estimated an extra variance component of 4.32 min, which was added in quadrature to the mid-transit times errors, and the following linear ephemeris:

$$T_0(E) = 2455392.3170(4)\mathrm{BJD_{TDB}} + E \times 1.430\,371\,48(53). \quad (5)$$

In this case, we obtained $\chi_r^2 = 0.32$. The O−C values computed from equation (5) are shown in the upper panel of Fig. 4. Here, it is possible to observe that considering an additional variance contribution of 4.32 min, the O−C data points are within the level of the error bars. To search for a periodicity in these data we ran two different tasks to the O−C values: a Lomb–Scargle (LS) periodogram (Horne & Baliunas 1986) and a Phase Dispersion Minimization (PDM) algorithm (Stellingwerf 1978) provided by IRAF. Both routines find very similar peaks at $P = 92.4$ epochs with a FAP[15] of 42 per cent for the LS periodogram (Fig. 5) and $P = 91.9$ epochs with $\Theta = 0.835$ for the PDM algorithm.[16] These high values for the false alarm probabilities and the absence of a clear periodic

case, it can be seen that the O−C data points show some substantial scatter, probably due to the magnetic activity of the host-star. To fully account for the stellar activity influence or any other remaining uncorrelated noise, we introduced an additional variance component (σ_s) in the ephemeris calculation. We estimated the value of this extra contribution using the same approach employed by Haywood et al. (2016, see their Section 4.1), who followed a procedure similar to the one described in Collier Cameron et al. (2006). This procedure basically consists in determining, through an iterative process, the value of σ_s that maximizes the likelihood ($\mathcal{L}$)

[15] FAP, for False Alarm Probability, is the probability that random noise produces a peak with power similar or higher than the one of the most significant peak in a certain period range. In this case, FAP was estimated through 10 000 MC simulations.

[16] Θ is a statistic that indicates how significant is the value found for a certain period. It is defined as $\Theta = s^2/\sigma^2$, where σ^2 is the variance of the analysed data series and s^2 is computed from the variances of data subsets obtained by splitting the original data series into several sub samples. If the found period is not true then $\Theta \sim 1$, while $\Theta \sim 0$ when the found period is correct. Note that $\Theta \sim 1$ and $\Theta \sim 0$ are equivalent to large and small values of FAP, respectively.

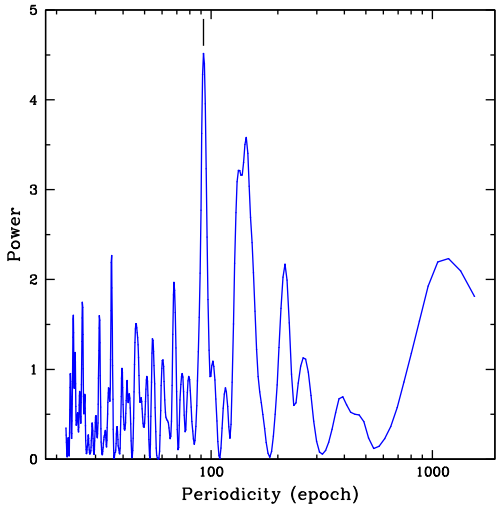

Figure 5. Lomb–Scargle periodogram of the O−C values corresponding to the 45 analysed light curves (continuous blue line). The most significant peak ($P = 92.4$ epochs) with FAP = 42 per cent is marked. Here, 'epoch' represents the number of transits since the minimum reference time shown in equation (5), while FAP (False Alarm Probability) is the probability that random noise produces a peak with power similar or higher than the one of the most significant peak in a certain period range. In this case, FAP was estimated through 10 000 MC simulations.

behaviour in the O−C data points seem to indicate that the period found around 92 epochs is not real. However, in the upper panel of Fig. 4 it is clear that some points strongly deviate from the predicted mid-transit times. We explored the causes of these departures looking for possible correlations between the O−C values and several indicators of the light-curve quality.

In Fig. 6, we plot the absolute values of O−C versus PNR (Fig. 6a) and β (Fig. 6b). Gibson et al. (2009) have demonstrated that the duration of the observations before/after the transit ingress/egress might play an important role in the normalization of the light curve and therefore in the determination of T_0. Bearing this in mind, we also plot in Figs 6(c) and (d), the $|O-C|$ values versus the duration of the out-of-transit observations before ingress (OOT_{ing}) and the out-of-transit observations after egress (OOT_{eg}), respectively. In all the plots, we distinguish between transits with PNR ≤ 3 and $\beta \leq 1.25$ (blue circles) and those with PNR > 3 and/or $\beta > 1.25$ (red triangles). The four light curves excluded from the ephemeris computation were also not considered in this analysis. For each figure, we performed a linear fit (solid line) to the data and computed the correlation coefficient r. We regarded $-1 < r \leq -0.8$ or $0.8 \leq r < 1$ as strongly, $-0.8 < r < -0.5$ or $0.5 < r < 0.8$ moderatly and $-0.5 \leq r < 0$ or $0 < r \leq 0.5$ weakly (positive or negative) correlated parameters. Taking this classification into account, no strong correlations between the absolute values of O−C and PNR, β, OOT_{ing} and OOT_{eg} are observed.

However, it is interesting to note that, with the exception of only one point, which corresponds to the epoch 561, the $|O-C|$ data points from the best quality transits (blue circles) do not exceed 2.4 min, whereas those derived from light curves of less quality (red triangles) show deviations up to 7.6 min. Moreover, mid-transit times errors are, on average, 4.34 and 4.51 min for the blue circles and the red triangles, respectively. These results would imply a possible connection between the transit quality and the calculated value of T_0 and its uncertainty. We investigated this possibility by plotting in Figs. 7(a) and (b) the errors in T_0 (e_{T_0}) versus PNR and β, respectively. In Fig. 7(b), we obtained a coefficient r of 0.447, which suggests a weak correlation between e_{T_0} and red noise. However, this correlation is fully dependent on the data point with a β factor of 3.3, which corresponds to the epoch 1316. If this transit is removed, r decreases to 0.062, showing almost no correlation between both quantities. On the other hand, in Fig. 7a we show with a solid line the best linear fit to the data points. In this case, we found a moderate correlation ($r = 0.672$) between the errors in the determination of the mid-transit times and PNR, suggesting that less quality light curves provide less accurate values of T_0.

Considering these results, we decided to re-calculate the ephemeris including only those light curves with mid-transit times uncertainties smaller than 1 min according to the values presented in Table 7 and no visible anomalies (Fig. 8). This reduced our sample to 31 transits spanning six complete years. By performing a maximum-likelihood analysis similar to that applied for determining equation (5), we obtained

$$T_0(E) = 2455392.3176(2)\mathrm{BJD_{TDB}} + E \times 1.430\,371\,23(26), \quad (6)$$

with $\chi^2_r = 0.83$. In this case, the estimated extra variance component added in quadrature to the errors in T_0, was 1.7 min. Contrary to the results obtained taking the 45 transits into account, an LS periodogram of the 31 data points does not show any significant peak, which confirms that the period of 92 epochs determined before is not real. This is in agreement with the finding by Ciceri et al. (2016), who did not find any periodic signal in the data. We also investigated if the use of different filters might affect the measurement of ephemerides. For the light curves corresponding to the nights of 2012 October 16 and 2013 April 24 observed with the GROND z' and g' filters, respectively, we repeated the fitting procedures explained in Section 3.2 and at the beginning of this section. However, this time, we took as initial values for the LD coefficients those corresponding to a different filter (the Johnson V filter). Then, we used the values and errors of the mid-transit times obtained from these fits and re-computed ephemeris, which was compared with that presented in equation (3). Given that the result of this comparison shows that the change in the ephemeris is within its 1σ error bars, we conclude that the ephemeris, and hence the measured mid-transit times, are not affected by the filters used to carry out the observations.

On the other hand, it is known that WASP-46 is an active star with a rotation period of 16 d, determined from the photometric variations produced by spots of magnetic origin (Anderson et al. 2012). Several works (Oshagh et al. 2013; Ioannidis, Huber & Schmitt 2016) caution that asymmetries in the light curves due to the passage of the planet in front of one or several spots during transit may lead to measure mid-transit times that strongly deviate from the predicted ones. Therefore, some of the outliers observed in Fig. 8, which deviate more than $\sigma = 1.66$ min from the predictions, can be due to anomalies during the transit produced by the presence of unseen stellar spots.

For completeness, we assessed if our standard deviation in the O−C data points might be compatible with the amplitude of the TTV expected by the Applegate effect[17] (Applegate 1992). According to equation (13) of Watson & Marsh (2010), this amplitude would be

[17] The Applegate effect is a mechanism that produces changes in the orbital period of the components of a binary system, due to quasi-periodic variations in the stellar quadrupole moment caused by magnetic activity cycles. This same effect is also expected to occur in planetary systems when the host-star is magnetically active (Watson & Marsh 2010).

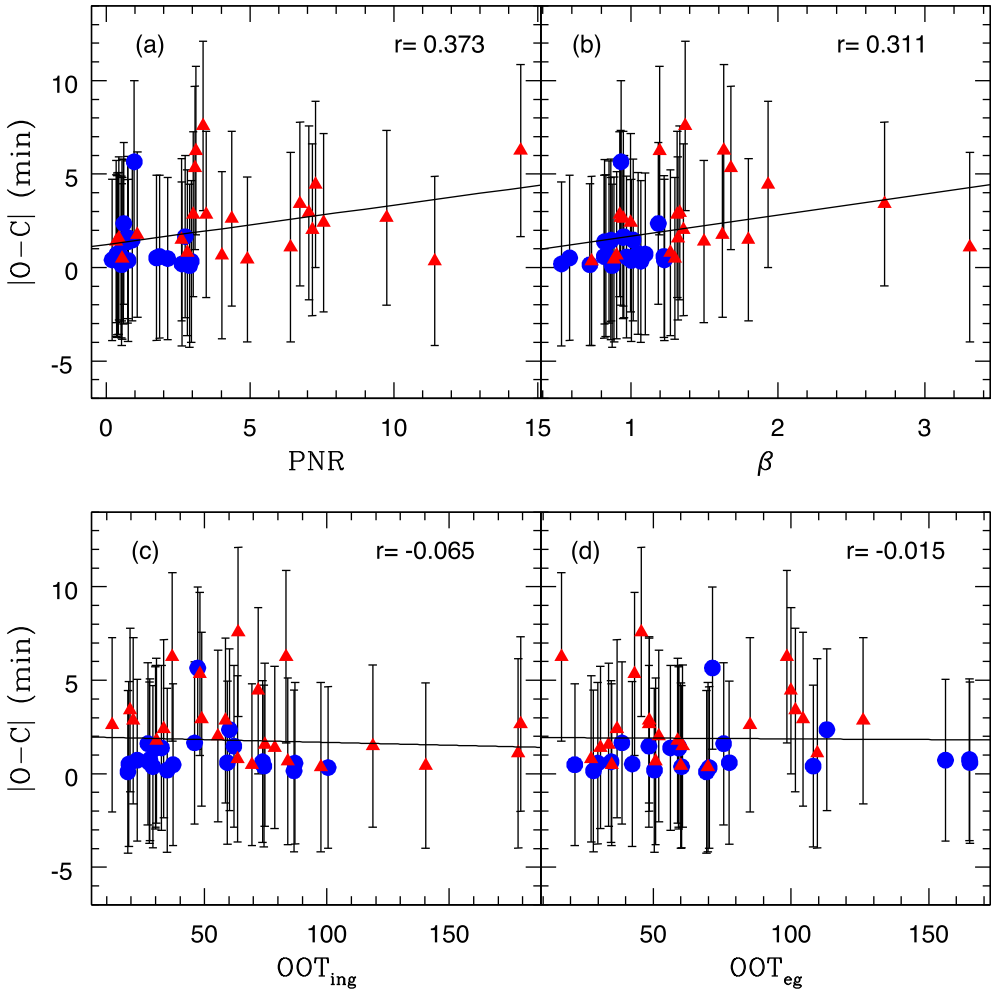

Figure 6. $|O - C|$ data points versus PNR, red noise (β), time before ingress (OOT_{ing}) and time after egress (OOT_{eg}). Here, PNR and β denote photometric accuracy of the light curves. Blue circles indicate high quality transits with PNR ≤ 3 and $\beta \leq 1.25$, while red triangles correspond to those poor quality light curves with PNR > 3 and/or $\beta > 1.25$. Solid lines represent the best fitting to the data and the r parameters are the correlation coefficients. We regarded $-1 < r \leq -0.8$ or $0.8 \leq r < 1$ as strongly, $-0.8 < r < -0.5$ or $0.5 < r < 0.8$ moderatly and $-0.5 \leq r < 0$ or $0 < r \leq 0.5$ weakly (positive or negative) correlated parameters. Taking this classification into account, no strong correlations between the $|O - C|$ values and PNR, β, OOT_{ing} and OOT_{eg} are observed.

of less than 1 s in 6 yr, which is far below the $\sigma \sim 1.6$ min found in our data. Hence, we can discard the variations in the quadrupole moment of WASP-46 as the cause of the observed dispersion in our mid-transit times.

Finally, using equation (33) of Agol et al. (2005) with the TTV dispersion determined for the 31 transits with e_{T_0} less than 1 min, we found that it is possible to exclude perturbers with masses larger than 2.3, 4.6, 7 and 9.3 $M_\oplus$ located in the positions of the first-order mean-motion resonances 2:1, 3:2, 4:3 and 5:4 with WASP-46b, respectively.

4.1 Analysis of long-term variations in transit depth and orbital inclination

The presence of a third body (exomoon, ring or another planet) in the system can also cause periodic variations in depth and/or orbital inclination. To study this possibility, we analysed the long-term behaviour of the photometric parameters k and i as a function of time for the 45 light curves without visible anomalies in their transits. To pursue this aim, we ran the JKTEBOP code individually on each light curve considering the depth, the scale factor, and the coefficients of the polynomial to fit the out-of-transit data points as free parameters, while the remaining ones were fixed to the values obtained in Section 3.2. We repeated the same procedure for the orbital inclination but, in this case, the sum of the fractional radii was also allowed to vary because i and Σ are correlated parameters. As before, we excluded from this study the incomplete light curve and the three light curves showing visible anomalies during the transit. In Fig. 9, we present our results. In both cases, we ran an LS periodogram and no significant peak was found in the data. However, for the k parameter some transits present depth values that depart from the standard deviation of the sample (here $\sigma = 0.0104$), similar to what we obtained for the mid-transit times. We suspect that these departures are consequence of the stellar activity present in WASP-46 (see e.g. Czesla et al. 2009; Croll, Rappaport & Levine 2015). Since our sample consists of light curves observed in 11 different filters, including wavelengths from 477 to around 914 nm, we extended the analysis performed by Ciceri et al. (2016) and explored the behaviour of the planetary radius as a function of wavelength. With this purpose, the 45 measurements of k were grouped together according to the filter in which they were observed. Then, for each data set we computed a weighted average of k and adopted as error

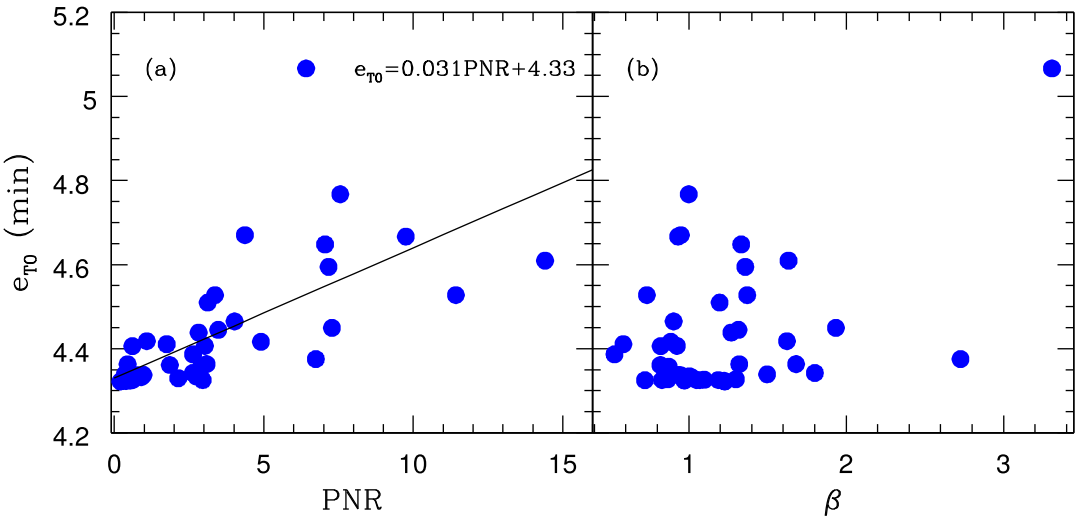

Figure 7. Uncertainties in mid-transit times (e_{T_0}) versus PNR (panel a) and β (panel b) factors. The black solid line represents the best fitting to the data points whose equation is indicated in the figure, and the r parameter is the correlation coefficient. For the data in panel b, we obtain $r = 0.447$ that suggests a weak correlation between e_{T_0} and red noise. However, this correlation is fully dependent on the data point with $\beta = 3.3$, which corresponds to the epoch 1316. If this transit is removed, r decreases to 0.062 showing almost no correlation between both quantities. On the other hand, for the data in panel a, we find a positive moderate correlation ($r = 0.672$) between the errors in the determination of the mid-transit times and PNR, suggesting that less quality light curves provide less accurate values of T_0.

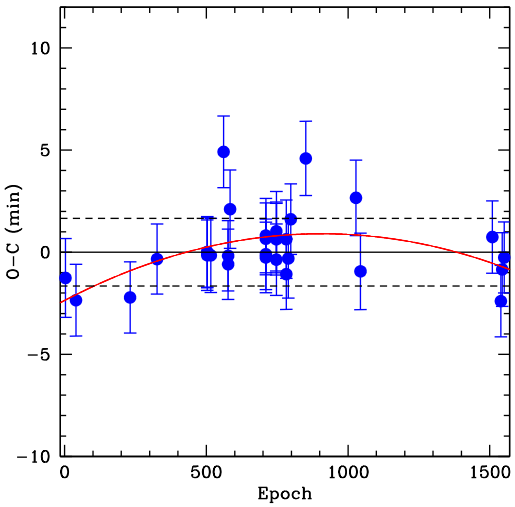

Figure 8. O−C data points versus Epoch. Here, O−C values are the observed mid-transit times minus the mid-transit times predicted using the ephemeris given by equation (6), while Epoch represents the number of transits since the minimum reference time shown in the same equation. We only plot the 31 light curves with uncertainties in their mid-transit times smaller than 1 min according to the values presented in Table 7. Dashed lines indicate $\pm\sigma$ ($\sigma = 1.66$ min) that represents the standard deviation of the data, while the red continuous line is the quadratic fit obtained from equation (11). Error bars include an additional variance component of 1.7 min, added in quadrature to the mid-transit times errors, which was computed from a maximum-likelihood approach.

its standard deviation. These values are shown in Table 8. By fitting a linear model through weighted least squares to this data, we obtained a slope $m = -0.98 \times 10^{-5}$ which is fully consistent with the value found by Ciceri et al. (2016). Assuming a scaling law for the cross-section of the dominant species given by $\sigma = \sigma_0(\lambda/\lambda_0)^{\gamma}$ (Lecavelier Des Etangs et al. 2008), the slope m will depend on the planet's atmospheric properties as follows:

$$m = \frac{\gamma T'_{\rm eq} k_{\rm B}}{\mu g_P}, \tag{7}$$

where $k_{\rm B}$ is the Boltzmann constant, μ is the mean molecular weight and $T'_{\rm eq}$ and $g_{\rm P}$ are the previously defined planet's modified equilibrium temperature and planetary surface gravity, respectively. Through the measured value of m, it is possible to determine if a scattering process is taking place in the planet's atmosphere and to infer which chemical component is producing it. However, we will not perform this kind of analysis because it is beyond the scope of this paper. In Fig. 10, we show the measured values of k and their errors as a function of wavelength. The linear model that best fits the data is indicated by a continuous black line. Furthermore, the upper panel of Fig. 9 shows that all the values of i agree, considering the errors, with the mean value measured for the orbital inclination.

4.2 Searching for a possible orbital decay

Considering the close proximity of WASP-46b to its host-star ($a \sim 0.024$ AU), it is interesting to study the possibility of orbital decay. According to Matsumura, Peale & Rasio (2010) planetary systems are 'Darwin unstable' (i.e. they have no tidal equilibrium states) when the ratio of the total angular momentum of the system ($L_{\rm tot}$) to some critical value ($L_{\rm crit}$) is lower than 1. Here,

$$L_{\rm tot} = L_{\rm orb} + (C_\star + C_{\rm P})n = \frac{M_\star M_{\rm P}}{\sqrt{M_\star + M_{\rm P}}}\sqrt{Ga(1-e^2)} + (C_\star + C_{\rm P})n \tag{8}$$

and,

$$L_{\rm crit} = 4\left(\frac{G^2}{27}\frac{M_\star^3 M_{\rm P}^3}{M_\star + M_{\rm P}}(C_\star + C_{\rm P})\right)^{1/4}, \tag{9}$$

where $L_{\rm orb}$ is the orbital angular momentum, G is the gravitational constant, $n = 2\pi/P$ the mean motion and $C = \alpha MR^2$ the moment of inertia. Using equations (8) and (9) for the system under study,

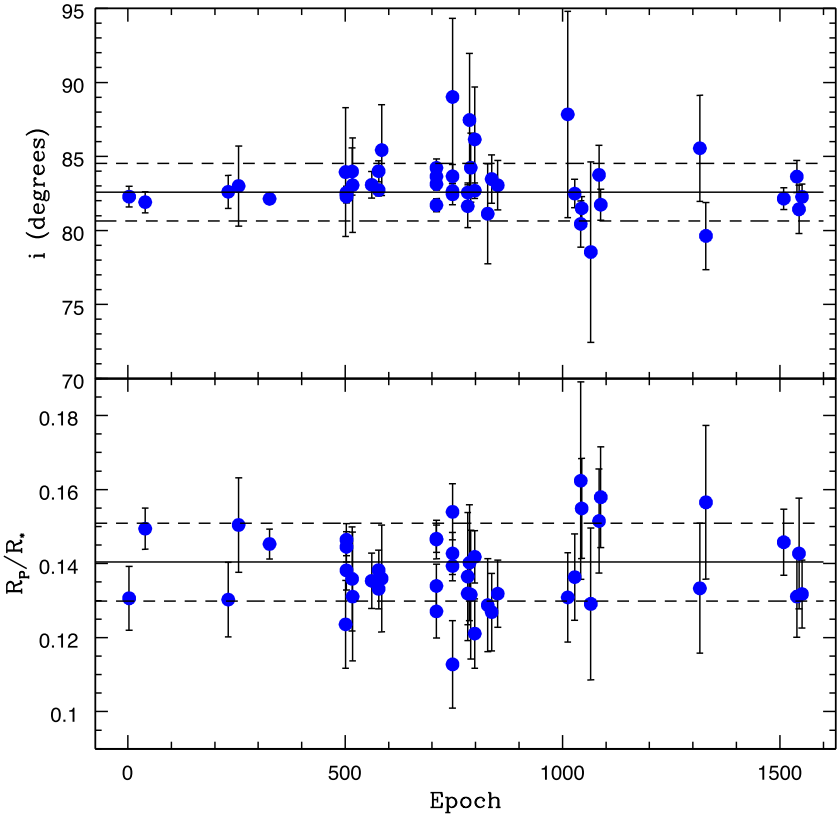

Figure 9. Long-term variations of i (upper panel) and k (lower panel). Here, Epoch represents the number of transits since the minimum reference time given by equation (4). Black solid lines indicate the weighted averages of the sample and dashed lines indicate $\pm\sigma$. Error bars are also shown.

Table 8. Average k values obtained for each filter.

Filter	λ_C (nm)	k	σ_k
GROND g'	477.0	0.1419	0.0026
Gunn g'	516.9	0.1452	0.0040
Jhonson V	551.0	0.1287	0.0125
clear	592.7	0.1361	0.0034
GROND r'	623.1	0.1442	0.0023
Jhonson R	640.7	0.1369	0.0039
Bessell R	648.9	0.1369	0.0043
Gunn r'	664.1	0.1449	0.0048
GROND i'	762.5	0.1317	0.0040
Cousins I+Sloan z'	849.9	0.1306	0.0086
GROND z'	913.4	0.1408	0.0031

Note. The λ_C values for the passbands 'clear' and 'Cousins I+Sloan z'' are the average λ_C of the Johnson V and the Cousins R filters, and the Cousins I and the Sloan z' filters, respectively.

we calculated $L_{\rm tot}/L_{\rm crit} \sim 0.11$[18] which means that the final fate of WASP-46b is to eventually fall on to the stellar surface. In this case, since e is nearly zero and the orbit is supposed to be synchronised, the tidal forces acting on the exoplanet can be considered negligible. However, since the stellar rotation period is larger than the orbital period, it is expected that tides continue to act on the host-star, decreasing the semimajor axis until the planet reaches its Roche limit ($a_{\rm R}$) and is tidally disrupted (Penev et al. 2012). According to Faber, Rasio & Willems (2005), the critical separation from which the planet starts to lose mass via its Roche lobe, $a_{\rm R}$, is given by

$$R_{\rm P} = 0.462 q^{1/3} a_{\rm R}, \tag{10}$$

where $q = M_{\rm P}/M_\star$ is supposed $\ll 1$. This relation between $R_{\rm P}$ and $a_{\rm R}$ is based on the Roche lobe radius determined by Paczyński (1971), who considered the classical stellar two-body problem supposing both stars as point masses in a circular orbit. In our case, adopting the stellar and planetary masses and the planet radius computed in Section 3.3, we found $a_{\rm R} = 0.009\,72$ AU. Assuming the current value of $a = 0.024\,07$ AU determined in this work, this result implies that WASP-46b has not crossed its Roche limit yet. However, we cannot rule out the possibility that the planet is losing mass through evaporation due to stellar radiation, given that this mechanism is not contemplated in the Roche limit calculation.

Orbital decay manifests as a systematic decrease of the orbital period. This implies that successive transits begin at times earlier than predicted ones, and therefore O−C values become systematically negative. The usual method to search for this shortening in the orbital period is to fit the mid-transit times with a quadratic and a linear ephemeris and compare which of both models better represents the data.

In this particular case, we performed a maximum-likelihood analysis to fit the mid-transit times corresponding to the 31 light curves for which $e_{\rm T_0} < 1$ min with the quadratic ephemeris equation of Adams et al. (2010)

$$T_0(E) = T_{\rm minref} + E \times P + \delta P \times \frac{E(E-1)}{2}, \tag{11}$$

[18] This value was computed considering the planet and the star as point masses ($\alpha = 1$ in both cases).

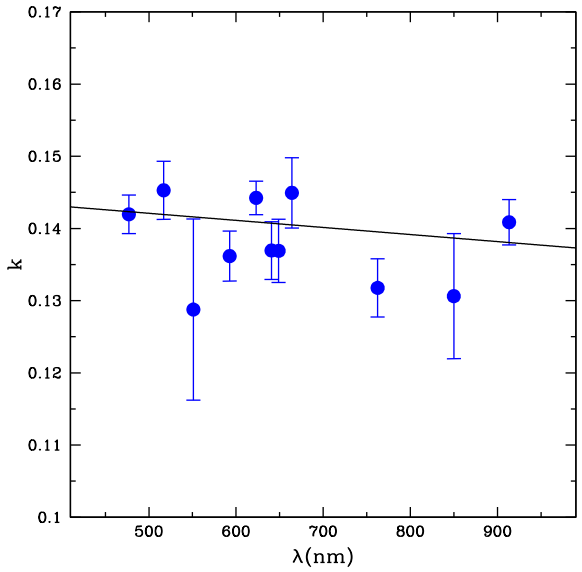

Figure 10. Variation of the transit depth of WASP-46b as a function of wavelength. Blue points are the average k values shown in Table 8 with their respective error bars. The black continuous line represents the linear model that best fits the data with a slope $m = -0.98 \times 10^{-5}$.

where $T_{\rm minref}$ is the reference minimum time and $\delta P = P \times \dot{P}$. In Fig. 8, the red continuous line represents the quadratic fit to the data. We obtained a variation of the orbital period per epoch (δP) of $(-5.41 \pm 2.25) \times 10^{-9}$ d and consequently a variation of the orbital period per year ($\dot{P}$) of -0.119 ± 0.049 s yr^{-1}. These small values for δP and $\dot{P}$ would be consistent with a constant orbital period. Following the methodology used in previous studies (see e.g. Chen et al. 2014a; Hoyer et al. 2016b), we applied to both the linear and the quadratic models the Bayesian Information Criterion (BIC) defined as,

$$\mathrm{BIC} = \chi^2 + k_{\rm FP} \ln N, \tag{12}$$

where $k_{\rm FP}$ is the number of free parameters for the adjustment and N is the number of data points. BIC is a useful tool to evaluate which of the fits better represents the data. In this sense, the best fitting will be the one with the lowest value of BIC. For WASP-46b, we obtained BIC = 33 for the linear model and BIC = 28 with a $\chi^2_{\rm r} = 0.56$ for the quadratic fit. These results indicate that a quadratic ephemeris is a better representation of the mid-transit times as a function of epoch. However, although we cannot rule out a possible slow decreasing rate of the period, we caution the reader that this evidence is still not significant and more observations are required before we can make conclusive statements on the orbital decay of the system.

Although the analysis presented above did not reveal any periodic variation in the mid-transit times or a significant shortening in the orbital period, the information obtained is useful to determine a lower limit on the tidal quality factor $Q_\star$. This parameter is related to the rate of tidal dissipation within the host-star and hence has an influence on the rate of orbital decay (Penev et al. 2012). Larger values of $Q_\star$ imply slower orbital evolutions. This points out the importance of this parameter in the theories looking to explain the formation of close in planets and their subsequent dynamic evolution. However, in spite of the theoretical effort put on the determination of $Q_\star$ (see e.g. Matsumura et al. 2010; Penev et al. 2012), the mechanisms of tidal dissipation in planets and stars are not well understood yet. Recently, several groups (Croll et al. 2015; Hoyer et al. 2016a,b; Maciejewski et al. 2016) have started to estimate the values of the tidal quality factor through observations of individual systems. We followed the procedure applied in these previous works and using a 1σ value based on our measured orbital decay, we adopted -0.07 s yr^{-1} as the upper limit of the estimated value for $\dot{P}$. Based on this number, we calculated $Q_\star > 7 \times 10^3$ for WASP-46 from equation (5) of Birkby et al. (2014). Although this value for the tidal quality factor is much lower than those normally assumed (between 10^5 and 10^{10}), it is physically plausible given that small values of $Q_\star$ have been also obtained in previous studies (see e.g. Adams et al. 2010; Blecic et al. 2014). Finally, we used the value of the lower limit determined for $Q_\star$ to compute a lower limit for the remaining lifetime of >0.34 Myr before WASP-46b falls on to the star.

5 SUMMARY AND CONCLUSIONS

In this work, we present 12 new transits of WASP-46b observed between 2012 and 2016. We use these observations and another 37 light curves collected from previous works and the ETD to redetermine the system's parameters and to compute new ephemeris. From the complete (full transit coverage) and higher quality light curves, we estimate photometric parameters that are in full agreement with the values published by Anderson et al. (2012), but are slightly different from those calculated by Kjurkchieva et al. (2015) and Ciceri et al. (2016), with the exception of k that is coincident in this last case. For the physical parameters, we find a value for the planetary radius consistent with the one computed in the discovery paper and somewhat larger than the one measured by Ciceri et al. (2016). Then, the main result of the first part of this work is that our estimations suggest a value for the planetary density between previous determinations by Anderson et al. (2012) and Ciceri et al. (2016).

We also perform the first homogeneous TTV study for this system over 6 yr of observations. For the 45 O−C data points corresponding to those light curves without visible anomalies during the transit, we get a dispersion of 2.61 min, although we do not find any periodicity. To explain this high value of σ, we search for possible correlations between $|O - C|$ and PNR, β, and the duration of the out-of-transit observations before ingress and after egress, but no significant correlation is detected. However, two interesting results arise from this analysis. First, best quality light curves (complete transits with PNR ≤ 3 and $\beta \leq 1.25$), with the exception of epoch 561, show $|O - C|$ values up to 2.4 min with an average error of 4.34 min, while transits of poor quality present $|O - C|$ values as much as 7.6 min with a mean error of 4.51 min. Secondly, we find a moderate correlation ($r = 0.672$) between the errors in the mid-transit times and PNR. This finding agrees with the results obtained in previous works and shows that poor quality transits imply not only less accurate values of T_0, but also larger errors. Since ephemerides are generally computed through weighted least squares, the values of P and reference minimum time are only slightly affected by poor quality light curves. However, these poor quality transits (often used in TTV's studies based on observations acquired with ground-based facilities) could mimic the variations in the O−C data points produced by another body. Therefore, caution must be taken when these low-quality observations are included in this kind of analysis.

Given that we showed that low-quality data usually provide less accurate values of mid-transit times with errors often underestimated, to calculate the ephemeris we only consider the 31 complete

light curves with errors in T_0 smaller than 1 min. In this case, we find a standard deviation of 1.66 min for the O−C data points, which is significantly smaller than the one obtained considering all the 45 data points. Since no periodic variation is detected in the data, we exclude the possibility that a second body gravitationally bound to the system can explain this result. We also discard the Applegate effect as a possible cause, since the amplitude of the variations produced by this phenomenon (less than 1 s) is significantly lower than the dispersion found (∼1.6 min). Alternatively, the high standard deviation we obtain can be due to stellar activity. In addition, our TTV dispersion allows us to exclude bodies with masses larger than 2.3, 4.6, 7 and 9.3 $M_\oplus$ at the first-order mean-motion resonances 2:1, 3:2, 4:3 and 5:4 with WASP-46b, respectively. Moreover, we do not detect any periodic behaviour in depth and orbital inclination for the 45 light curves. Several values of k differ more than $\pm\sigma$ from the mean value, probably due to the effect of unseen stellar spots in the light curves.

Given the short distance between WASP-46b and the star, we also search for a possible orbital decay. Through the computation of the total angular momentum of the system, we conclude that the planetary orbit is unstable and WASP-46b will eventually spiral in towards its host-star. We also estimate that the planet has not crossed its Roche limit yet. Furthermore, we find that a quadratic fit to the 31 best mid-transit times is a better (BIC = 28) representation of the data than the linear model (BIC = 33), which prevents us from ruling out the possibility that the orbital period of WASP-46b might be decreasing. However, from the quadratic model we estimated small values for $\delta P = (-5.41 \pm 2.25) \times 10^{-9}$ d and -0.119 ± 0.049 s yr^{-1}, suggesting that if a decay in the planetary orbit is actually taking place, the variation rate of the period is very low. Moreover, it is important to mention that even considering a typical light-curve precision of 2×10^{-3} and 6 yr of observations, our results cannot significantly demonstrate a slow decrease of the orbital period of WASP-46b. Hence, this trend is not conclusive and needs to be confirmed by extending the baseline of transit observations. This value of $\dot{P}$ allows us to compute a lower limit on the tidal dissipation coefficient of $Q_\star > 7 \times 10^3$. On the other hand, according to equation (7) of Birkby et al. (2014) and assuming our current light-curve precision and O−C dispersion of 1.6 min as the expected transit time shift, we would be able to rule out values of $Q_\star < 10^5$ after six additional years of transit observations. Given that there is still no clear evidence to decide if the orbit of the planet is decaying or not, the transfer of angular momentum from the planetary orbit to the stellar surface proposed by Maxted et al. (2015) remains a possibility that might explain the discrepancy between the gyrochronological and isochronal ages.

ACKNOWLEDGEMENTS

R P and E J acknowledge the financial support from Consejo Nacional de Investigaciones Científicas y Técnicas (CONICET) in the form of postdoctoral fellowships. R P also thanks to Dr Simona Ciceri for kindly providing the light curves of her work. R P and E J are also grateful to the operators of the 1.54-m telescope at EABA, Cecilia Quiñones and Luis Tapia, for their support during the observing runs, and to Estefanía Vendemmia for observing the transit of 2014 August 22. R P thanks Martin Mašek for nicely providing information about the observations of WASP-46b published in the ETD. The authors acknowledge support from the PIP 2013–2015 GI 11220120100497 of CONICET (Argentina). This research has made use of the SIMBAD database, operated at CDS, Strasbourg, France and NASA's Astrophysics Data System. We also thank the referee for a thorough review of the manuscript and constructive comments and suggestions, which improved the content and quality of the paper. This work is partially based on observations obtained with the 1.54-m telescope at Estación Astrofísica de Bosque Alegre dependent on the National University of Córdoba, Argentina. Partially based on observations made with ESO telescopes at the La Silla Paranal Observatory under programme ID 60.A-9022(A).

REFERENCES

Adams E. R., López-Morales M., Elliot J. L., Seager S., Osip D. J., 2010, ApJ, 721, 1829
Agol E., Steffen J., Sari R., Clarkson W., 2005, MNRAS, 359, 567
Anders E., Grevesse N., 1989, Geochim. Cosmochim. Acta, 53, 197
Anderson D. R. et al., 2012, MNRAS, 422, 1988
Applegate J. H., 1992, ApJ, 385, 621
Birkby J. L. et al., 2014, MNRAS, 440, 1470
Blecic J. et al., 2014, ApJ, 781, 116
Chen G., van Boekel R., Wang H., Nikolov N., Fortney J. J., Seemann U., Wang W., Mancini L., Henning T., 2014a, A&A, 563, A40
Chen G., van Boekel R., Wang H., Nikolov N., Seemann U., Henning T., 2014b, A&A, 567, A8
Ciceri S. et al., 2016, MNRAS, 456, 990
Claret A., 2000, A&A, 363, 1081
Collier Cameron A. et al., 2006, MNRAS, 373, 799
Croll B., Rappaport S., Levine A. M., 2015, MNRAS, 449, 1408
Czesla S., Huber K. F., Wolter U., Schröter S., Schmitt J. H. M. M., 2009, A&A, 505, 1277
Demarque P., Woo J.-H., Kim Y.-C., Yi S. K., 2004, ApJS, 155, 667
Eastman J., Siverd R., Gaudi B. S., 2010, PASP, 122, 935
Faber J. A., Rasio F. A., Willems B., 2005, Icarus, 175, 248
Fressin F., Guillot T., Nesta L., 2009, A&A, 504, 605
Fulton B. J., Shporer A., Winn J. N., Holman M. J., Pál A., Gazak J. Z., 2011, AJ, 142, 84
Gibson N. P. et al., 2009, ApJ, 700, 1078
Girardi L., Bressan A., Bertelli G., Chiosi C., 2000, A&AS, 141, 371
Gonzalez G., Vanture A. D., 1998, A&A, 339, L29
Haywood R. D. et al., 2016, MNRAS, 457, 3637
Horne J. H., Baliunas S. L., 1986, ApJ, 302, 757
Howell S. B., 1989, PASP, 101, 616
Hoyer S., Palle E., Dragomir D., Murgas F., 2016a, Astron. J, 151, 137
Hoyer S., López-Morales M., Rojo P., Minniti D., Adams E. R., 2016b, MNRAS, 455, 1334
Ioannidis P., Huber K. F., Schmitt J. H. M. M., 2016, A&A, 585, A72
Jofré E., Petrucci R., Saffe C., Saker L., de la Villarmois E., Artur C. C., Gómez M., Mauas P. J. D., 2015a, A&A, 574, A50
Jofré E., Petrucci R., García L., Gómez M., 2015b, A&A, 584, L3
Kjurkchieva D., Petrov N., Popov V., Ivanov E., 2015, Bulga. Astron. J., 22, 21
Kurucz R., 1993, ATLAS9 Stellar Atmosphere Programs and 2 km s^{-1} grid. Kurucz CD-ROM No. 13. Smithsonian Astrophysical Observatory, Cambridge
Lecavelier Des Etangs A., Pont F., Vidal-Madjar A., Sing D., 2008, A&A, 481, L83
Maciejewski G. et al., 2016, A&A, 588, L6
Mallén-Ornelas G., Seager S., Yee H. K. C., Minniti D., Gladders M. D., Mallén-Fullerton G. M., Brown T. M., 2003, ApJ, 582, 1123
Matsumura S., Peale S. J., Rasio F. A., 2010, ApJ, 725, 1995
Maxted P. F. L., Serenelli A. M., Southworth J., 2015, A&A, 577, A90
Oshagh M., Santos N. C., Boisse I., Boué G., Montalto M., Dumusque X., Haghighipour N., 2013, A&A, 556, A19
Paczyński B., 1971, ARA&A, 9, 183
Penev K., Jackson B., Spada F., Thom N., 2012, ApJ, 751, 96
Petrucci R., Jofré E., 2016, Boletín de la Asociación Argentina de Astronomía, 58, 298
Petrucci R., Jofré E., Schwartz M., Cúneo V., Martínez C., Gómez M., Buccino A. P., Mauas P. J. D., 2013, ApJ, 779, L23

Petrucci R., Jofré E., Melita M., Gómez M., Mauas P., 2015, MNRAS, 446, 1389
Pietrinferni A., Cassisi S., Salaris M., Castelli F., 2004, ApJ, 612, 168
Poddaný S., Brát L., Pejcha O., 2010, New A, 15, 297
Pollacco D. L. et al., 2006, PASP, 118, 1407
Saffe C., 2011, RMxAA, 47, 3
Sneden C. A., 1973, PhD thesis, Univ. Texas
Southworth J., 2009, MNRAS, 394, 272
Southworth J., 2010, MNRAS, 408, 1689
Southworth J., 2012, MNRAS, 426, 1291
Southworth J., Maxted P. F. L., Smalley B., 2004, MNRAS, 351, 1277
Southworth J., Wheatley P. J., Sams G., 2007, MNRAS, 379, L11
Stellingwerf R. F., 1978, ApJ, 224, 953
Stetson P. B., 1990, PASP, 102, 932
Watson C. A., Marsh T. R., 2010, MNRAS, 405, 2037
Winn J. N. et al., 2008, ApJ, 683, 1076
Zhou G., Bayliss D. D. R., Kedziora-Chudczer L., Tinney C. G., Bailey J., Salter G., Rodriguez J., 2015, MNRAS, 454, 3002

SUPPORTING INFORMATION

Supplementary data are available at *MNRAS* online.

Table 2: Photometry of WASP-46 obtained in this work.

Please note: Oxford University Press is not responsible for the content or functionality of any supporting materials supplied by the authors. Any queries (other than missing material) should be directed to the corresponding author for the article.

This paper has been typeset from a TEX/LATEX file prepared by the author.